KUNGLIGA TEKNISKA HÖGSKOLAN

Master in Engineering physics

Reactor Physics

Master Thesis

First principle calculations of the residual resistivity of defects in metals

Giulio Imbalzano

Supervisors:

Dr. Pär Olsson

Dr. Carlo Enrico Bottani

Abstract

The materials of a nuclear power plant are subject to extreme conditions during the lifetime of a reactor and therefore must be thoroughly studied. The variation of the microstructure will affect the macroscopic properties which in turn can lead to accidents. Several experimental techniques can be used to study and predict the lifetime behaviour of the materials such as the isochronal annealing experiments that have been among the first to be performed. As theory progressed and increasing computational power was available it became even possible to simulate such experiments on computers and several successful examples are now available but the research can still be refined. A simple relation has always been used for the residual resistivity variation which was never investigated.

An ab-initio study has therefore been performed to analyse the variation of the residual resistivity depending on the crystalline configuration of defects using Density Functional Theory (DFT) and Boltzmann theory. Two methods have been applied to cross check the results and comparison to experimental values has shown satisfactory agreement. Two materials have been thoroughly investigated, iron and tungsten, due to their importance in the nuclear industry. The results have shown that different effects may take place which negate a purely linear relation between the number of defects and the residual resistivity for both iron and tungsten. A previous study on the topic was also re-analysed in light of the results obtained within this work. However, only a quantitative difference has been found whereas the general behaviour of the results remains unchanged.

Sammanfattning

Vissa komponenter I kärnkraftverk utsätts för extrema förhållanden under reaktorns livstid och bör därför studeras noggrant. Förändringar I mikrostrukturen påverkar makroskopiska egenskaper, vilket I sin tur kan leda till olyckor. Många experimentella tekniker kan användas för att studera och förutspå beteendet av material, en av dessa är isokron anlöpning. Med vidareutvecklad teori och kraftfullare datorer är det nu möjligt att simulera dessa experiment. Det finns för närvarande många exempel på lyckade simuleringar, men modellerna kan fortfarande förfinas. Hittills har endast enkla modeller för den residuella resistiviteten använts, och försök till att implementera förbättringar av dessa modeller har aldrig gjorts.

En ab-initio-undersökning har därför utförts med syftet att analysera variationer i den residuella resistiviteten beroende på konfigurationen av kristalldefekter med hjälp av täthetsfunktionalteori (DFT) och Boltzmannteori. Två metoder har tillämpats för att erhålla resultat, och jämförelse med experimentella värden har visat god överensstämmelse. Två material har undersökts ingående, järn och wolfram, p.g.a deras betydelse i kärnkraftsindustrin. Resultaten visar att olika effekter kan äga rum vilka leder till en avvikelse från en rent linjär relation mellan antalet defekter och den residuella resistiviteten, både i järn och wolfram. En tidigare studie av ämnet har återanalyserats med hänsyn till resultat från denna undersökning. En kvantitativ skillnad har funnits, medan de allmänna slutsatserna är oförändrade.

Acknowledgements

First of all I would like to thank my supervisor, Pär. You have provided me a fantastic opportunity and I can hardly thank you enough. Thanks to you I have tasted what research feels like, a spoonful of despair and a hint of joy, and, what is more, I have been able to do it in a great environment. You have been supportive and helpful and you have shown me a glimpse of the world in which I would like to live in my future. And, mostly, you have done all of this treating me as a person.

Then I would like to thank everyone in the department, Luca, Antoine, Karl, Zhongweng, Elin, Janne, for the interesting conversations at lunch and during the small breaks in the day. They have helped me to get through the days, even when nothing looked right.

Thanks to Chiara, Francesco and Anna for taking care of me during this year. It has been a pleasure to meet you and I have enjoyed the time spent together.

Thanks to all the people from Tyresö, which I will not forget anytime soon. Raffaello, especially, you have been my landmark whenever I felt lost and started wondering what I was doing.

I will not forget those who are 6000 km far away, in Italy, and the long distance support you have given me. Nicolò, Riccardo, Sergio, Stefano, you have made me feel that I was never truly alone and always welcome home.

All the people from Politecnico, those from the bachelor and those from the master. And from high school, and from judo and everybody else whom I forgot. I truly believe that all of you have helped me being what I am today and a bit of you is here, in this work.

To my dear Elisabetta, thanks for accepting my selfishness, for your patience and all your love. You never failed to let me know that you are there and that I can rely on you. Thank you.

Finally, to my family. Thanks for the joy, the support and the love. Thanks for the patience that you had and the affection that you never failed to convey. Even Gabriele, despite living on other side of the planet. This work is dedicated to all of you as a small token of my appreciation for what you have done.

Most of the computer simulations have been performed on the resources provided by the Swedish National Infrastructure for Computing (SNIC) at PDC.

Contents

List of Figures

List of Tables

Chapter 1

Introduction and Motivation

1.1 Introduction

In metallurgy many different techniques have been used throughout the decades in order to study materials, investigate their microstructure, their macroscopic properties and how these two are related. It is known that defects in the matrix can affect greatly the properties of the material and therefore it has always been of interest to find methods to characterize these defects. A multitude of techniques have been developed, making use of various phenomena such as quantum tunnelling, diffraction, but also simple resistivity measurements.

An industry which makes extensive use of this knowledge is the nuclear one. Nuclear power plants (NPPs) produce an important share of the electricity in the world and an increase may even be considered to reduce the production of carbon dioxide. However, safety is the primary concern in such facilities, therefore the research to reduce risks and increase the capabilities of NPPs is still ongoing and probably never-ending. Among others also the materials deserve a special focus because the conditions created inside a nuclear power plant are unique and among the most extreme known. What makes the environment so hostile is a combination of rather high temperatures (with peaks of almost 350 °C during normal operation), mechanical and thermal stress, high concentration of corrosive agents and a very high neutron flux. This last element is particularly important as it increases by a significant factor the amount of defects present in the materials.

Focusing only on the steels in the NPP it is possible to characterize different

materials, such as austenitic stainless steels (SS) used in cladding and internal parts, low alloy steels for the Reactor Pressure Vessel (RPV), body centred cubic (bcc) Fe-Cr alloys used in the primary system and ferritic/martensitic steels which are considered to be the best candidates for IV generation reactors [1] also containing oxides to strengthen the steel [2]. Therefore a big experimental effort is needed to be able to investigate properly the microstructure of each of these materials and how this determines the macroscopic properties. It is known that the defects in the material affect the swelling, the ductility, the thermal conductivity and other properties of the material but their response greatly varies depending on many parameters, difficult to study separately.

The theory has evolved at the same pace as experiments in order to verify and study the experimental results and now models are available to simulate the kinetics of the defects inside the materials through methods such as atomic kinetic Monte Carlo (AKMC) and object kinetic Monte Carlo (OKMC). These methods yield results precise enough to be compared to the experiments but they are adjusted to the theories which rely heavily on the experimental data. Therefore when different methods used to investigate the microstructure yield different results, problems arise. In [3–5], for example, small angle neutron scattering (SANS) and atom probe tomography (APT) yield different results regarding the composition of the precipitates after irradiation. In other cases, such as isochronal annealing experiments [6, 7], results are found but assumptions must be made to understand them properly. In all of these cases the theories and the models at hand can possibly be used to verify the source of discrepancies or the origin of some data, given that the models are good enough to represent the experiments.

Focusing on this last cited method, the isochronal annealing with resistivity recovery measurements, many materials have been investigated through the years for a better comprehension of their microscopic structure. These relatively simple experiments have been used since the fifties in order to study the kinetics of the defects and are still an interesting source of data. Nowadays, however, it has become possible to simulate these very same experiments on a computer using ab initio Density Functional Theory (DFT) methods together with Monte Carlo simulations as in [8, 9] in order to improve the analysis. In the first reference Fu and co-workers have reached results comparable to the experiments and her work has been used to validate the assumptions that had been accepted for half a century

regarding the kinetic of the defects in Iron. This has shown how much theories and computational instruments have evolved to the point of being able to complement experimental data.
In her work, however, a simple assumption has been made to calculate the resistivity, that is that single defects contribute equally to the resistivity independently from their aggregation, i.e. a cluster of n vacancies has the same effect of n independent vacancies. This assumption derives from the fact that modelling the resistivity is no easy task and much work is needed in order to obtain significant results. In a work from Clouet [10] a simple relation is used for resistivity of scandium solutes in aluminium but only the dependence of resistivity on the cluster dimension is considered and the data are taken from experiments. Effort has been placed to compute the resistivity using first principle methods for several different systems, such as sodium [11–13], aluminium [11, 14, 15], iron [16] and others. Although giving good results, these calculations have the drawback of demanding a significant amount of computational power which increases dramatically as the temperature decreases because bigger and bigger cells are required to have convergent results [16]. This is also the reason why the majority of the referenced papers deal with the liquid form of the corresponding element.

On the other hand most microstructural changes occur at low temperature and to model isochronal annealing experiments this knowledge is necessary. Therefore different models have been investigated to simulate the electrical resistivity for defected systems at low temperature. The Boltzmann theory of transport has been used to calculate electrical resistivity at room temperature in materials containing defects, such as vacancies or solutes [17–19] with good results. Different approaches can be taken towards the solution of the Boltzmann equation, each with its own advantage and drawback, but it has been shown that interesting results have been found even for spin-dependent systems, such as iron and cobalt [20] at temperatures varying from 0 K to several hundreds K.

1.2 Aim of the work

The aim of this work is to try to complement the current knowledge about the resistivity of defected systems possibly becoming a reference for further research by setting up a simple and easy-to-reproduce method for calculating these quantities.

Basic models have been used until now, as in the work of Fu [9], or calculations have been run for single systems, within other studies. However, at this moment it is thought that the possibility of investigating thoroughly the topic exists and must be attempted.

First of all it would be interesting to verify if the models proposed by Fu or Clouet actually hold starting from first-principle calculations or if they are too simplistic and should be improved upon. The objective is not to question their results, most of which would hold whatever the outcome of this thesis, but to complement them and propose better methods for future research.

This work is also interesting to question how far the models have advanced and if computer simulations are capable of investigating phenomena that are not fully available from experiments. In order to validate theories, experiments are necessary and generally they are run in extreme conditions to study one quantity at a time. But despite the incredible steps forward in the theories, the models are usually kept simple. This becomes a limiting factor in the field here considered because it is difficult to study how single defects affect the resistivity. Therefore some assumptions must be made but they limit how far it is possible to properly study the topic. For example a common assumption is that during isochronal experiments the defects are originally created singularly. So, if the number of defects can be estimated using other theories, it is possible to calculate how single defects contribute to the resistivity. However, starting from first principle calculation it is possible to investigate the effect of a single defect and estimate their contribution to the total resistivity.

Chapter 2

Theoretical Background

This part of the thesis is written to provide a general background on the physics and the methods that have been used for this work. The first topic will be an introduction to the crystal structure and the defects that can be found in it, followed by an overview of the isochronal annealing experiments and their usefulness in the study of the behaviour of defects. The modelling methods that have been used to study the resistivity recovery will then be presented and explained, from the theory to their implementation in the codes. The first topic introduces is DFT, which provides essential information that can be used as an input for other models. Then the focus will be placed on the different theories of transports that have been developed over time and that are used within this work in order to estimate the conductivity of the chosen materials and that make use of the output from the DFT calculations.

Atomic units are used in this chapter unless specified.

2.1 Crystal structure and defects

2.1.1 Crystal structure

The crystal structure describes the manner in which the atoms are spatially arranged. The atoms of a crystalline solid tend to self-organize in highly ordered structures due to the symmetric nature of the bonds that they can form. In the crystalline lattice a unit cell can be identified, which is the smallest structure that

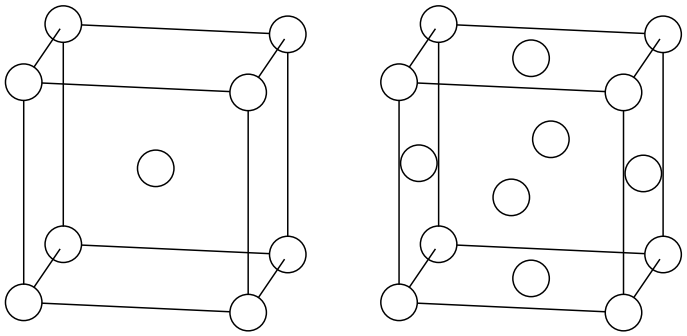

(a) (b)

Figure 2.1: The atomic configurations of a BBC (Fig. a) and FCC (Fig. b)

repeats by translation in the crystal without overlapping.

Given the intrinsic difference among atoms, it is clear that not all of them will have the same structure, although some simple and common ones can be identified. Most metallic atoms adopt one of three basic structures: the body centred cubic (BCC), the face centred cubic (FCC) and the hexagonal close packed (HCP), two of which are shown in figure 2.1.

2.1.2 Defects

A crystalline defect is a region where the local arrangement of ions differs from that of a perfect crystal. Several defects can be distinguished and they are generally classified by the dimension, spanning from 0 (point defects) to 3 (bulk defects). In this work the focus will be placed on 0D defects, as they are the main topic of study in DFT simulations where the dimension of the cell is not large enough to include bigger defects and because they constitute the main defects caused by irradiation. A brief review of these will follow.

A lattice site which should have been filled with an ion but instead is left empty is called a vacancy. The surrounding crystal structure is stable enough to avoid that the crystal will collapse on the void left, but some re-organization is expected in order to cope with the different electronic density.

On the other hand, an atom can be found in a position that should have been otherwise empty and this is called an interstitial defect. It is possible to observe both Self Interstitial Atoms (SIA), where the extra atom is of the same type of

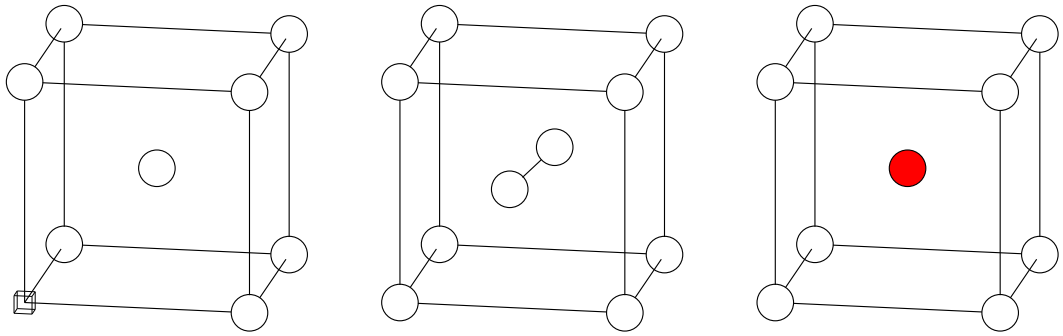

(a) (b) (c)

Figure 2.2: Three point defects illustrated in a BCC structure. Figure (a) shows a vacancy in position (0 0 0), Fig. (b) a dumbbell SIA along the [110] direction and Fig. (c) shows a substitutional atom in the central position.

the lattice, or Foreign Interstitial Atoms (FIA) if it is an alien specie. The former tend to occupy the same lattice site of another atom, thus creating a dumbbell structure, whereas the latter can usually be found in octahedral or tetrahedral sites in between the other atoms.

A foreign atom which occupies a normal lattice site is generically referred as a substitutional defect. Examples of these three point defects can be seen in figure 2.2. It must be noted that all of these defects can be present at the same time and it is not unusual that they will interact among themselves. For example, two vacancies that come too close to each other will form a di-vacancy, whereas interstitial and vacancies can recombine destroying each other. The di-vacancy is of particular interest as it will move and behave as a different entity compared to two single vacancies.

Depending on the position of the second vacancy with respect to the first, we will be referring to x^{th} nearest neighbour (xnn), where x identifies the distance from the first site, as shown in figure . Sometimes the concept of a far away divacancy will be used. This indicates that the second vacancy is placed in the furthest position available in the configuration. In direct coordinates this can be expressed saying that the vacancies are placed at (0 0 0) and (.5 .5 .5).

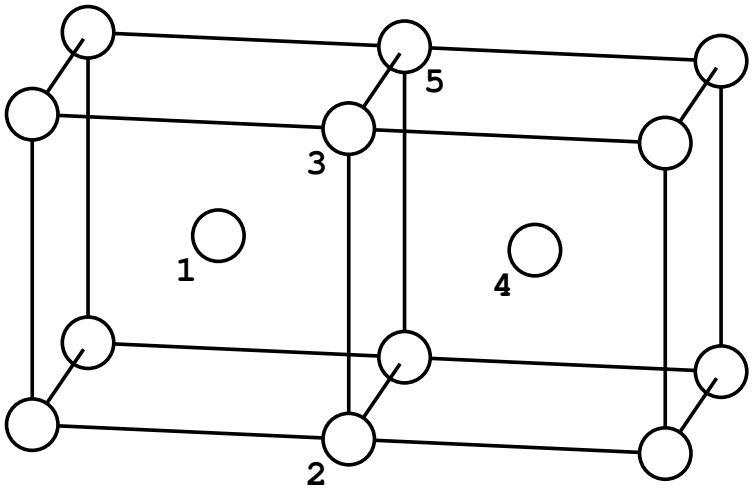

Figure 2.3: The 5 nearest neighbours to the atom in position (0 0 0) in a BCC lattice

2.1.3 Generation of defects

Point defects are always present in crystals at thermal equilibrium and thus a perfect crystal does not normally exist. The probability that enough energy to cause a point defect is gathered due solely to local fluctuations is finite. This can be shown rather easily starting from the Gibbs free energy function G applied to a system of N atoms with n defects. The basic idea is that the presence of defects increases the entropy of the crystal and thus G is minimized for a non-zero n at finite temperature [21, 22]. The n/N ratio will indeed be very small, but not zero.

In the presence of radiation the number of point defects can be greatly increased. This is due to the fact that the average energy of the radiation is usually

several orders of magnitude higher than the threshold displacement energy of the atoms (MeV against eV), therefore each radiation-matter interaction (neutrons against steel in the case of a Nuclear Power Plant) will contribute to the creation of several defects, mainly Frenkel pairs (combination of a vacancy and an interstitial). Most of these will recombine, but the remaining ones will affect the properties of the material.

2.2 Isochronal annealing

Isochronal annealing is one of the first techniques used by scientist to investigate the defects in a material. The experimental set-up is rather simple compared to the complexity of the problem that it allows to investigate. In this case it is related to the resistivity recovery that will be treated within this same section for brevity.

A typical experiment of interest in the nuclear industry consists in the irradiation of a material whose composition is known (pure materials, alloys or materials with known concentrations of impurities are commonly used) at a certain, usually low, temperature. Later the material is heated following a precise and regular scheme; the temperature is raised by a fixed amount and kept constant for a certain time (whence "isochronal"). It is thus expected that the defects caused by the radiation, as explained in section 2.1.3, will begin diffusing in the material and be destroyed (annealed) by interacting with other defects, e.g. the recombination of a Frenkel pair. The basic idea is that the defects will begin diffusing at different temperatures, thus it is possible to study the energy needed by each one to begin migrating. Such experiments have permitted to study the kinetic and the dynamics of the defects even in times when modern technologies were not yet available.

In order to ascertain the annealing of the defects, the resistivity of the material is measured. In particular it is assumed that each defect will contribute to a raising of the resistivity due to the change in the electronic configuration in the metal as

$$\Delta\rho = \sum_i c^i \rho_D^i \tag{2.1}$$

where c^i is the concentration of a type of defect and ρ_D^i the resistivity contribution. Therefore when a defect gets annealed and disappears from the material a decrease

in the resistivity is expected to be seen. The exact number of defects that have actually annealed is unknown but it is known that a certain type of defect (SIA, vacancies etc.) has started diffusing at that temperature.

With the knowledge obtained from such experiments it is possible to evaluate the radii of interaction of the defects, the activation enthalpy of migration and much more.

2.2.1 Isochronal annealing in modelling

These experiment have not been abandoned despite the advent of much more sophisticated methods that have been developed from the '50s till today. It has become of particular interest also to model the experiments in order to be able to verify certain hypothesis that had been made in the past. For example Fu and co-workers [9] have been able to verify the order in which the defects begin moving in iron using only first principle and kinetic Monte Carlo calculations. Within their work the necessity to simulate the resistivity was faced through the use of a very simple method. It was simply assumed that the resistivity depends solely on the number of defects and not on their configuration.

2.3 Density Functional Theory

This theory has been developed in order to be able to solve the Schrödinger equation (Eq 2.2 shows the time-independent form which will be treated within this section) for cells bigger than a few atoms and in a rather small amount of time. Despite the many approximations that can be used, trying to solve directly the Schrödinger equation remains too expensive from a computational point of view. The problem is also not easily solved by increasing computational power because it lies in the exponential scaling between time and number of electrons.

$$H\Psi(x_1, x_2, ...) \; = \; E\Psi(x_1, x_2, ...) \tag{2.2}$$

In this equation x= (r, σ), where r is the coordinate and σ the spin. The Hamiltonian operator, H, can be written as a sum of three terms

$$H = T + V_{ee} + V_{ext} \tag{2.3}$$

where T is the kinetic energy of electrons, V_{ee} is the electron-electron interaction and V_{ext} is the interaction with the external potential, which in the context of material simulation and as a consequence in this thesis, is the interaction between electrons and nuclei. It must be noted that two terms have been neglected following the Born-Oppenheimer approximation [23] which states that due to their significantly heavier masses, the nuclei move much slower than the electrons. The consequence is that the electrons will be considered to be moving in a field of still nuclei and thus the kinetic energy of the nuclei is close to zero and their interaction contributes with a constant to the Hamiltonian.

The only constraints needed to solve equation 2.2 are that Ψ must be antisymmetric and normalized. For every wavefunction Ψ that can be inserted in equation 2.2 it is possible to calculate the average total energy E as

$$E[\Psi] = \int \Psi^* \hat{H} \Psi dr \equiv \langle \Psi | \hat{H} | \Psi \rangle \tag{2.4}$$

and by the variational principle (Eq 2.5) this will be greater than the ground state energy E_0.

$$E[\Psi] \geq E_0 \tag{2.5}$$

Out of all the possible wavefunctions, the one which minimizes the total energy will be taken, which is the ground state wavefunction. The ansatz proposed by Hartree-Fock is an antisymmetric and normalized product of functions ψ_i each depending on only one electron out of the N present in the system.

$$\Psi(x_1, x_2, ..., x_N) = \frac{1}{\sqrt{N!}} \begin{vmatrix} \psi_1(x_1) & \psi_2(x_1) & \cdots & \psi_N(x_1) \\ \psi_1(x_2) & \psi_2(x_1) & \cdots & \psi_N(x_1) \\ \vdots & \vdots & & \vdots \\ \psi_1(x_N) & \psi_2(x_1) & \cdots & \psi_N(x_1) \end{vmatrix} \tag{2.6}$$

Substituting the ansatz in the Schrödinger equation gives the Hartree-Fock equations,

$$\left[-\frac{1}{2}\nabla^2 + v_{\text{ext}} + \int \frac{\rho(r')}{|r - r'|} dr' \right] \Phi_i(r) + \int v_{\text{x}}(r, r') \Phi_i(r') dr' = \epsilon_i \Phi_i(r) \tag{2.7}$$

$$\int v_{\text{x}}(r, r') \Phi_i(r') dr' = -\sum_j^N \frac{\Phi_j(r) \Phi_j^*(r')}{|r - r'|} \Phi_i(r') dr' \tag{2.8}$$

where v_x is the non local exchange potential.

This is, however, not the final step, but the first one in the direction of a more precise answer through better approximations (correlated methods) that unfortunately require huge computational power. The main problem, as it was mentioned beforehand, lies in the scaling of the computational time, which follows the number of electrons raised to the power of 5 to 7 [24]. Therefore applying this method to systems of hundreds of electrons is clearly unreasonable. Hence DFT was developed and applied.

2.3.1 The Hohenberg Kohn (HK) theorems

Two theorems were proved and published by Hohenberg and Kohn in 1964 [25]. The first can be expressed as follows;

"The electron density determines the external potential (to within an additive constant)"

This has important consequences for equation 2.3 because now the electron density determines every term of this equation. Thus knowing the charge density it becomes possible to determine the Hamiltonian and all the related properties. The second theorem can be expressed as follows;

"For any positive definite trial density ρ_t, such that $\int \rho_t(r)dr = N$, then $E[\rho_t] \geq E_0$."

This means that given the charge density at ground state it is possible to determine the ground state energy. From the second theorem we can deduce that if the charge density contains the correct number of electrons, then it is possible to determine the ground state energy and density as the minimum of a functional $E[\rho]$. This functional is universal (independent from the external potential of the system) and, if known, would yield the exact ground density and energy.

Going back to the Schrödinger equation it can be seen that the energy functional is a sum of three terms,

$$E[\rho] = T[\rho] + V_{ext}[\rho] + V_{ee}[\rho] \tag{2.9}$$

which are the same as Eq 2.3, but it is now specified their functional dependence on ρ. The interaction with the external potential is the easiest term to find, but two more are missing and must be approximated. The better the approximation, the better results this method yields.

2.3.2 Kohn and Sham

In order to solve this problem, an interestingly simple solution was proposed by Kohn and Sham. A new system, with the same electron density is defined, but in this case no interaction among the electrons is considered and a new external potential is introduced to make up for the error [26]. The kinetic energy of a non-interacting system of electrons with the same ground state density as the original case can be written as

$$T_s[\rho] = -\frac{1}{2}\sum_{i}^{N}\langle\Phi_i|\nabla^2|\Phi_i\rangle \tag{2.10}$$

$$\rho(r) = \sum_{i}^{N}|\Phi_i|^2 \tag{2.11}$$

Out of the whole electron-electron interaction, a significant part will be made up of the classical Coulomb interaction, which can be written as

$$V_H[\rho] = \frac{1}{2}\iint\frac{\rho(r_1)\rho(r_2)}{|r_1 - r_2|}dr_1dr_2 \tag{2.12}$$

where the H stands for Hartree, as this is also called the Hartree energy within this context. Now the energy functional can be rewritten taking into account this term and the self-interaction correction needed to correct the equation.

$$E[\rho] = T_s[\rho] + V_{ext}[\rho] + V_H[\rho] + E_{xc}[\rho] \tag{2.13}$$

The exchange-correlation functional $E_{xc}[\rho]$ is unknown and makes up for all the errors arising from calculating the kinetic energy without interactions (here called T_s) and by treating the electron-electron interaction classically (neglecting spin and self-interaction, thus the only term V_H). Therefore it is possible to write it as a sum of two errors, as follows

$$E_{xc}[\rho] = (T[\rho] - T_s[\rho]) + (V_{ee}[\rho] - V_H[\rho]) \tag{2.14}$$

where T and V_{ee} are the kinetic energy and the electron-electron interaction of the interacting system. It must be noted that, despite this quantity being called exchange-correlation functional it contains also terms related to kinetic energy and is not only the sum of exchange and correlation terms as it was in the Hartree-Fock equation.

In light of this, it is now possible to rewrite the Hartree-Fock equation 2.7 and derive the Kohn-Sham equation as follows.

$$\left[-\frac{1}{2}\nabla^2 + \nu_{ext}(r) + \int \frac{\rho(r')}{|r-r'|}dr' + \nu_{xc}(r)\right]\phi_i(r) = \epsilon_i\phi_i(r) \tag{2.15}$$

The exchange-correlation potential ν_{xc} replaces the non-local exchange potential from the Hartree-Fock equation and it can be written as

$$\nu_{xc}(r) = \frac{\delta E_{xc}[\rho]}{\delta\rho}. \tag{2.16}$$

The solution of the energy problem now becomes self-consistent: starting with a reasonable guess for the density, it becomes possible to calculate all of the functional quantities and construct new orbitals (Eq 2.15). From these a new density is available (Eq 2.11) and can be compared to the starting one. This cycle is repeated until convergence between the initial density and the calculated one is found.

It must be noted that the computational power needed to solve the Kohn-Sham equation should scale with N^3 but in reality it is possible to reduce the scaling factor towards N^1 by exploiting the locality of orbitals at least for certain simple systems, such as insulators [24].

Only one problem is now left, that is the calculation of the exchange-correlation energy. If this was known exactly, then the whole method would yield exact results. Unfortunately this is not possible, thus approximations are needed and several methods have been proposed.

The Local Density Approximation

A first attempt to calculate the exchange-correlation energy is the so called Local Density Approximation (LDA) which is strongly interconnected to the Thomas-Fermi gas model of the 1920s. This method is based on the idea that the exchange-correlation energy can be computed considering only the local electronic density. Therefore one easy choice is to apply the homogeneous electron gas (HEG) model proposed by Fermi and Thomas and calculate E_{xc}. By linearly decomposing the exchange-correlation energy in its two terms as $E_{xc} = E_x + E_c$, it becomes rather easy to find an expression for the exchange term within the HEG model. This is, in fact, for a non-interacting homogeneous electron gas

$$E_x[\rho] = 0.74\int \rho^{4/3}(r)dr \tag{2.17}$$

Analytical results for the correlation density are unknown but for the high and low density limit. For intermediate values can either be estimated by quantum Monte Carlo simulations which yield accurate results [27] or by interpolating the values obtained in such simulations.

Despite the many approximations, this model gives surprisingly good results. This is, however, mostly due to a cancellation of errors in the exchange and correlation density, which are generally underestimated and overestimated respectively, giving in average a good result [24]. Better methods have been developed which do not increase drastically the computing time.

The Generalized Gradient Approximation

A second approach to compute the exchange-correlation energy is to consider not only the relation to the charge density but also to its derivative. If this was applied directly to the charge density, several non-physical effects would arise. Thus a functional form is adopted which forcibly ensures the normalization condition and that the exchange hole is negative. This functional can be described with the following equation.

$$E_{xc} = \int \rho(r)\epsilon_{xc}(\rho, \nabla\rho)dr \tag{2.18}$$

The Perdew-Burke-Ernzerhof (PBE) GGA functional deserves a special mention. Here all the parameters are fundamental constants, making it easier to derive, understand and improve [28]. The numerical results are only slightly better than the Perdew-Wang 1991 (PW91) functional, but some limits of the previous work are overcome in this one. Almost all of the simulations that have been run within this thesis have made use of this exchange-correlation functional. This approximation gives better results if compared to the LDA, but it has still been refined over the time by accounting for the second derivative of the electron density (Meta-GGA functionals) or by mixing several of these functionals in a parametric way (Hybrid Exchange Functionals).

2.3.3 The Wavefunction

After determining a form for the exchange-correlation energy, with all of the possible approximations, it is now important to have a good representation of the

wavefunction for each atom. Two requirements must be satisfied, that is to be realistic and computationally inexpensive.

Norm-conserving pseudopotentials

One possibility is to express the wavefunction with plane waves as follows.

$$\Phi_i(r) = \sum_K c_{i,K} e^{i(k+K)\cdot r} \tag{2.19}$$

This approach is suitable for slowly varying wavefunctions. However, in the core region of the atom the wavefunction is rapidly oscillating, thus requiring a huge number of plane waves to have a convergent basis set. This is solved by considering the atom to be divided in two parts. One is the core region, populated by core electrons, which are considered to be frozen and unimportant with respect to the interaction with the other atoms. The outer part is populated by valence electrons, which are responsible for the bonding and the other properties of the atom. So it is possible to describe with the plane waves only the valence electrons, giving to the core region a smoothed potential needed to reach faster convergence. The choice of the core radius, r_c, impacts on the convergence (softness) and on the accuracy of the pseudopotential in different situations (transferability).

To conserve the transferability, pseudo wavefunctions are usually chosen to be norm-conserving, i.e.

$$\int_0^r |\tilde{\Psi}(r)|^2 dr = \int_0^r |\Psi(r)|^2 dr \tag{2.20}$$

for $r < r_c$. In some cases, however, not even this requirement is enough to have a computationally efficient basis set, so some corrections were done and Vanderbilt [29] proposed a set of ultra-soft pseudopotentials which needed a very small basis set. However, other methods have been developed with time, with more accurate results.

Projector Augmented-Wave

This method mixes the previous pseudo-potential and the augmented wave (which has not been treated here, but it can be found in [Martin R.M.]) methods. In the valence region, the same approach that has been described for pseudopotential is

used. In the inner zone, on the other hand, atomic orbitals are used to describe the wavefunction.

Auxiliary (smooth) wavefunctions chosen to be easily expanded into plane waves, are introduced by a linear transformation operator, T as

$$|\Psi_i\rangle = \hat{T}|\tilde{\Psi}_i\rangle \tag{2.21}$$

where Ψ_i represents the real wavefunction and $\tilde{\Psi}_i$ is the smooth one. The transformation operator can be written as

$$\hat{T} = 1 + \sum_R S_R \tag{2.22}$$

where S_R is the difference between the smooth and the real wavefunction and it is made so that it acts only inside the core radius r_c. Outside it vanishes smoothly at the boundary and leaves only the identity matrix (here written as 1) outside this sphere, called usually augmentation sphere. R represents the site of the nuclei.

Inside this core region, using the frozen core approximation, it is possible to expand the smooth wavefunction using auxiliary partial wave states $|\tilde{\phi}_j\rangle$, where the index j accounts for the position (R) and the partial wave. The smooth partial waves can also be written as

$$|\phi_j\rangle = (1 + S_R)|\tilde{\phi}_j\rangle \tag{2.23}$$

and outside the augmentation sphere, since only the identity matrix remains, the following is true:

$$|\phi_j\rangle = |\tilde{\phi}_j\rangle. \tag{2.24}$$

It is now possible to introduce smooth projector functions $|\tilde{p}\rangle$ (related to the expansion coefficients which couple the wavefunctions Ψ_i to the partial waves ϕ_j) and rewrite the transformation operator as

$$\tilde{T} = 1 + \sum_k (|\phi_k\rangle - |\tilde{\phi}_k\rangle)\langle\tilde{p}_k|. \tag{2.25}$$

The projector functions are required to satisfy orthogonality conditions inside the augmentation sphere. Finally, it is possible to relate the real wavefunction with the auxiliary as

$$|\Psi_i\rangle = |\tilde{\Psi}_i\rangle + \sum_j (|\phi_j\rangle - |\tilde{\phi}_j\rangle)\langle\tilde{p}_j|\tilde{\Psi}_i\rangle. \tag{2.26}$$

2.3.4 Vienna Ab-initio Simulation Package

Most of the DFT calculations within this thesis have been performed using the Vienna Ab-initio Simulation Package (VASP). The potentials used are PBE with the Projector Augmented Wave method. Simulations have been run for both iron and tungsten, with rather similar input parameters. The cut-off energy for the two materials has been set to 300 eV as suggested from the potential files used and extensive convergence tests.

Given the periodic boundary conditions used by the program, it is important to have a big enough cell to avoid image interaction effects, i.e. the defect in the cell must not interact with itself in the next periodic cell. Cells of 128 and 250 atoms have been used for this purpose, for both iron and tungsten, whereas bigger cells have been used for comparison and testing purposes. Also various k-point grids have been tested but ultimately, due to symmetry problems when the VASP output was interfaced with BoltzTraP, low-symmetry k-point grids have been chosen. The convergence has been tested using 3x3x3 grids to 7x7x7 with no symmetry (flag ISYM = 0 in the INCAR). The calculations have been run with a number of k-points in the irreducible Brillouin zone between 100 and 200. These were chosen taking the k-point grid of the crystallographic configuration with the lowest symmetry and running the other calculations with the same grid. Relaxation of the cells has been run with less dense k-point grids (usually 3x3x3 for 250 atoms and 5x5x5 for 128 atoms) and the resultant positions of the atoms have been used as input for denser grids.

2.3.5 ABINIT

ABINIT has been used for more DFT calculations, but mainly for the Density Functional Perturbation Theory (DFPT, described in y.y) implemented in the code. The initial objective of using this program as a comparison for the VASP+BZTP calculations has met some problems since they are very computationally demanding and the number of configurations that could be investigated was consequently limited. More effort will be placed in this direction for improving this work.

ABINIT has shown remarkably good results in the calculations for the resistivity on the materials when using 12x12x12 k-point grids and equally spaced q-point

grids. For tungsten and other test materials even less dense grids could have been used with low errors, but these values have been set as standards given the good average results. The energy cut-off has been set to 16 Ha (435 eV) for tungsten and 32 Ha (870 eV) for iron. Tolerances of 10^{-24} have been set for the mean squared residuals of the wavefunctions. The position of the nuclei in the defected cells has been relaxed using VASP and transferred to ABINIT.

In this case GGA norm-conserving pseudopotentials have been used because DFPT for GGA-PAW methods has not been implemented yet.

2.4 Electron transport theory

Starting from the 1900, three years after the discovery of the electron by Thomson, several models trying to explain the electrical and thermal conductivity have been developed. As a deeper understanding of atomic structure as well as quantum physics was reached, the models were modified to take into account the new discoveries. Within this chapter some of the possible methods used to calculate the resistivity will be reviewed. For a deeper understanding of the topic, however, more comprehensive texts are recommended, such as [21] and [30].

2.4.1 Drude model

Just 3 years after the discovery of the electron, Drude tried to apply the successful kinetic theory of gases to this new particle. The basic assumption is that the electrons are seen as molecules free to move inside the box, undergoing collisions among themselves. In this case the electrons are free to move inside the metal but the collisions are assumed to happen not among themselves but between electrons and ions (which at the time where unknown, but Drude assumed they were some kind of neutral background entity making up most of the matter). The electrons are assumed to be both independent and free, that means that other than the collision event, no other interaction is assumed to exist with other electrons or between electrons and ions. The collisions are instantaneous events which cause the variation of the velocity of the electrons. The exit velocity is assumed to depend only on the temperature of the ions and is completely independent of the incoming one. This brings one more approximation, that is that a single collision is sufficient

to bring the electrons to thermal equilibrium with the ions in the surroundings. An average time between collisions, called relaxation time or mean free time, τ is postulated and implies that the probability of an electron undergoing a collision in a time dt is equal to dt/τ.

All of these are very strong assumptions and most of them have been proven wrong, but within a certain limit they still hold. The "electron gas", free and independent, is not a bad approximation for the electrons in a metal, usually completely unbounded from the neutral background of ions and core electrons. The idea of a collision between electrons and ions, as well as the relaxation time approximation, are basic assumptions also of more modern models, such as the Boltzmann theory. The difference is that the classical idea of an electron bouncing off an ion has been completely abandoned after a better understanding of these particles has been available. This model, despite the big amount of critics that can be moved, has shown some good results in particular for some families of atoms, such as alkali metals and noble metals [21].

The relation between the current density and the electric field can be expressed through the use of the conductivity σ as

$$j = \sigma E. \tag{2.27}$$

This equation represents the first step towards the calculation of the conductivity in the classical model. In the following equations the resistivity ρ may be used instead of the conductivity but the two quantities are the reciprocal of one another as

$$\rho = \frac{1}{\sigma}. \tag{2.28}$$

The objective now is to rewrite σ as a function of known quantities through classical mechanics. A number n of electrons is assumed to have velocity $\vec{v}$ and travel a distance equal to vdt in a time dt in the direction of $\vec{v}$. A total of $n(vdt)A$ electrons will pass through an area A and each electron has a charge equal to $-e$. Therefore the total charge crossing A is $-nevA\,dt$ and the current density is

$$\vec{j} = -ne\vec{v}. \tag{2.29}$$

After a collision the electron is supposed to have a velocity $\vec{v_0}$ directed in a random direction, so in the absence of electric fields the average velocity of all the electrons

$\vec{v}$ is assumed to be 0. However, if a field is present, the velocity of an electron at a time t after a collision will be $\vec{v_0} - e\vec{E}t/m$, where the second term accounts for the acceleration given by the electric field. The average of this quantity, remembering that the average of t is τ, will be

$$\vec{v}_{avg} = -\frac{e\vec{E}\tau}{m}. \tag{2.30}$$

The current density is thus simply

$$\vec{j} = \left(\frac{ne^2\tau}{m}\right)\vec{E} \tag{2.31}$$

and straightforwardly the conductivity is

$$\sigma = \frac{ne^2\tau}{m}. \tag{2.32}$$

It is then possible to extract the relaxation time τ, assuming that the resistivity ρ is known from experiments, by inverting the previous formula as

$$\tau_D = \frac{m}{\rho n e^2}. \tag{2.33}$$

The number of electrons contributing to the conduction n has not been treated until now because it is a source of problems. The simplest possibility is to consider the number of atoms per cubic centimetre and assume that each contributes with Z conduction electrons to the total. The value of Z can be assumed to be the number of valence electrons, but ambiguity remains for all of those elements having more than one chemical valence. This problem was not faced directly but another solution was adopted, as explained in section 2.4.3.

2.4.2 Boltzmann theory of transport

To describe the conduction a non-equilibrium distribution function $g_n(r, k, t)$ will be used. This is defined so that $g_n(r, k, t)drdk/4\pi^3$ is the number of electrons in the nth band at time t in the phase space volume $drdk$ about the point r, k. At equilibrium, $g_n^0(r, k, t)$ is the Fermi function but, as it was stated, here g will be considered to be perturbed by an electric field (in a more complete treatment also a temperature gradient should be considered, but it is of no interest in this case).

The first step is to consider a semiclassical motion of the electron, having a velocity $v_n(k)$ and subject to a forcefield F as follows,

$$v_n(k) = \frac{1}{\hbar}\frac{\partial}{\varepsilon_n(k)} \tag{2.34}$$

$$F = -e[E(r,t) + \frac{1}{c}v_n(k) \times H(r,t)] \tag{2.35}$$

where $\varepsilon_n(k)$ represents the energy for a given band index n, depending on the wave vector k, and H is the magnetic field, which will later be neglected. Given this, it is possible to write a conservation equation of g. Considering an infinitesimal time dt, it is straightforward that an electron at r, k at time t must have been at $r - v(k)dt$, $k - Fdt/\hbar$ at time $t - dt$. Introducing also the possibility of collisions (without specifying what kind), the conservation equation takes the form

$$\begin{aligned} g_n(r,k,t) = g_n(r - v(k)dt, k - \frac{Fdt}{\hbar}, t - dt) \\ + \left[\frac{\partial g_n(r,k,t)}{\partial t}\right]_{out} dt + \left[\frac{\partial g_n(r,k,t)}{\partial t}\right]_{in} dt \end{aligned} \tag{2.36}$$

where $[...]_{out}$ is the correction related to electrons which get scattered and fail to arrive in r, k at time t and $[...]_{in}$ accounts for the electrons which managed to reach that point only because of a previously unaccounted collision. From here on the dependence on the band, time and position will be omitted for simplicity, leaving only the wave vector k. 2.36 can be rewritten in differential form as

$$\frac{\partial g(k)}{\partial t} + v(k) \cdot \frac{\partial g(k)}{\partial r} + \frac{F}{\hbar} \cdot \frac{\partial g(k)}{\partial k} = \left(\frac{\partial g}{\partial t}\right)_{coll} \tag{2.37}$$

where the left part takes into account the motion of electrons and the right one the collisions. The term F accounts for both electric and magnetic field, but the latter will be neglected. The electric field will bring the system to a steady-state situation, where the derivative of the function g with respect to time is 0. Therefore the equation now is composed of only two terms, that is

$$v(k) \cdot (-e)\frac{\partial g(k)}{\partial \varepsilon_k} E = \left(\frac{\partial g(k)}{\partial t}\right)_{coll} \tag{2.38}$$

where the right term can be rewritten using the relaxation time approximation, that is

$$\frac{\partial g(k)}{\partial t} = \frac{g^0(k) - g(k)}{\tau_k}. \tag{2.39}$$

The relaxation time τ_k is the average time between two collisions which will alter the momentum k and/or the band index n of the electron. The nature of the collision is left unknown and more appropriate models redefine this quantity in a more precise way [21]. However, within this work and the programs used, this approximation is acceptable.

The last effort requires to consider the steady-state as a small perturbation of the equilibrium function, that is $g(k) \approx g^0(k)$ where $g^0(k)$ is nothing else than the Fermi function. This brings, finally, an expression for the distribution function $g(k)$ as

$$g(k) = g^0(k) - \tau_k v(k) \cdot (-e) \frac{\partial g^0(k)}{\partial \varepsilon_k} E. \tag{2.40}$$

The distribution function $g(k)$ can be used as well to write the current density of a single band as

$$j = -\frac{e}{\Omega} \int v(k) g(k) dk \tag{2.41}$$

where Ω is the volume. Combining equations 2.27, 2.40 and 2.41, it is possible to write the conductivity of a single band as

$$\sigma^{(n)} = \frac{e^2}{\Omega} \int \tau_{n,k} v_n(k) v_n(k) \frac{\partial g^0(k)}{\partial \varepsilon_k} dk \tag{2.42}$$

and the sum of all the conductivities for each band will become the conductivity tensor

$$\sigma = \sum_n \sigma^{(n)}. \tag{2.43}$$

It must be noted that within the Boltzmann theory τ has not been defined. With the information at hand it is possible to calculate the quantity σ/τ but no more than this. Within some approximation it is possible to state that the relaxation time is independent of the band index n and the wave vector k, therefore stating that it is constant. However, in this work this approximation has shown some limitations, therefore the aforementioned Drude model has been used to estimate τ.

2.4.3 BoltzTraP

Many DFT programs give, in the output, the energy bands. It is possible to make use of this output to extrapolate even more properties of the material, such as

σ/τ that was introduced in section 2.4.2. BoltzTraP [31] is one such code, able to calculate from the energy bands other information (among others the Seebeck and Hall coefficients, as well as the electronic contribution to the thermal conductivity, and more). Within this work the interest was mainly the aforementioned σ/τ which was later converted to a value of the resistivity simply as

$$\rho = \frac{1}{\frac{\sigma}{\tau}\tau_D}. \tag{2.44}$$

As it was discussed before, the quantity τ_D was taken using the Drude model. It must be noticed that in this case the relaxation time will not be independent of the temperature as it is commonly considered. A relation between τ and the temperature is known to exist, but is usually disregarded for simplicity. In this case, however, a constant τ would have given acceptable results only around the room temperature, whereas a more realistic model was desired. Anyway, this is not a source of errors, as it will be explained later on, because the objective of this work is to compare the difference in resistivities of different crystallographic configurations, which depend solely on the σ/τ given by the program. Also, the density of conducting electrons was considered to be constant and fitted in order to have the same resistivity of the experimental data at 150 °C. This procedure is similar to that used in other works, such as [17, 19].

Since the code needs a huge number of k-points for correct computation of the transport quantities, the band energies are interpolated using a Fourier expansion. The term lattice points is used instead of k-points to express the extrapolated points and the ratio of lattice-points/k-points can be chosen by the user. Star functions are used in order to avoid to modify the space group symmetry. Between two band energies the interpolating curve also minimizes a roughness function to avoid oscillations that could have strong influence on the results. More about the code can be found in [31] and in the manual present in the code itself. A VASP-to-BoltzTraP program was already available and used for this work. A modification was done to process also ferro-magnetic materials such as iron. The VASP output file containing the eigenvalues for both spins was read and stored in two different input files (named energiesup and energiesdn) to be used in BoltzTraP separately. It is possible that additional modifications may be necessary as well as a deeper understanding of the code.

Since the cells used within this work are mainly non-fully-symmetric it has

been decided to use space group (1) for all the calculations. It is believed that different symmetries could be used for each cell but several problems, related to what has been explained in section 2.3.4, have lead to choose the space group (1) for all of the configurations. The lattice-points/k-points ratio has ultimately been chosen to be 5. In older simulations the results showed great variation depending on the lattice-points/k-points ratio. Convergence was achieved with a ratio of 40 but the following results showed unphysical behaviour. When less symmetric k-point grids were used in VASP, however, the dependence of the σ/τ with the lattice-points/k-points ratio was completely lost and therefore a small ratio of 5 was used. The ratio, however, does not appear to impact significantly on the computational power needed for the BoltzTraP calculations.

2.4.4 Density Functional Perturbation Theory

The method that has been described until now, that is to calculate the quantity σ/τ through the Boltzmann equation and τ with the Drude model, is not fully ab initio and uses a parameter, the density of conduction electrons, to fit the experimental data. However, this method is very cost efficient and therefore has been used extensively in this work. On the other hand fully ab initio methods exist and are available but consume enormous amount of computational resources and thus must be carefully used. The Density Functional Perturbation Theory (DFPT, can also be called linear response theory) is one such method that has also been used in this work. A complete treatment of the theory would require a lot of time, space and mathematics, so a shorter, but hopefully exhaustive, treatment will follow. A simple way to see it would be to say that the relaxation time τ introduced in section 2.4.1 and 2.4.2 is here analytically calculated considering only the electron-phonon interaction, which is the dominant effect on the electron lifetime at intermediate temperatures [30].

The objective is to evaluate how the electron-phonon interaction will perturb the electronic Hamiltonian. Within the DFPT, the phonon spectra and the electron-phonon interaction are evaluated using the first order variations caused by the presence of a phonon with wave vector q in the one-electron wavefunctions, the charge density and the effective potentials. So the objective is to evaluate the

electron-phonon matrix element

$$g^{q\nu}_{k+qj',kj} = \langle k+qj'|\delta^{q\nu}V_{\text{eff}}|kj\rangle \tag{2.45}$$

where $q\nu$ is the mode of the phonon with which the electrons are interacting and both ψ_{kj} and $\psi_{k+qj'}$ have the Fermi energy ϵ_F. The change in the potential can be written as

$$\delta^{q\nu}V_{\text{eff}} = \sum_{R,\mu} \frac{\eta_{q\nu}(R\mu)}{(M_R\omega_{q\nu})^{1/2}} \frac{\delta^+ V_{\text{eff}}}{\delta R_\mu} \tag{2.46}$$

where M_R are the masses of the nuclei, $\eta_{q\nu}(R\mu)$ are the eigenvectors of the $q\nu$ mode and $\omega_{q\nu}$ is the phonon mode interacting with the electrons.

However, expression 2.45 must be corrected to account for the incompleteness of the basis functions. The Fermi golden rule is here used to study the scattering rate of electrons to a perturbed state $\tilde{\psi}_r(t)$ from an unperturbed one $\psi_s(t)$ due to phonons. From here on the method will only be discussed and the results presented; the mathematical steps can be found in Ref [32].

The time-dependent Schrödinger equation is written for both the perturbed and unperturbed state and the wavefunctions are evaluated using a variational method as in the Linear Muffin Tin Orbital method as follows

$$\psi_s(t) = \sum_\alpha \chi_\alpha A^s_\alpha(t). \tag{2.47}$$

The two Schrödinger equations are expanded up to the linear term and after some calculations an expression for the scattering rate is found through the Fermi golden rule. It is now possible to rewrite the electron-phonon matrix element accounting for the incomplete basis set as

$$g^{q\nu}_{k+qj',kj} = \langle k+qj'|\delta^{q\nu}V_{\text{eff}}|kj\rangle + \langle \sum_\alpha \delta^{q\nu}\chi^{k-q}_\alpha A^{k+qj'}_\alpha | H-\epsilon_{kj}|kj\rangle + \langle k+qj|H-\epsilon_{k+qj}|\sum \delta^{q\nu}\chi^k_\alpha A^{kj}_\alpha\rangle \tag{2.48}$$

and use it to find the phonon line width $\gamma_{q\nu}$ using again the Fermi golden rule

$$\gamma_{q\nu} = 2\pi\omega_{q\nu}\sum_{kjj'} |g^{q\nu}_{k+qj',kj}|^2 \delta(\epsilon_{kj}-\epsilon_F)\delta(\epsilon_{k+qj'}-\epsilon_F). \tag{2.49}$$

The electron-phonon spectral distribution function is written in terms of the phonon line width as

$$\alpha^2F(\omega) = \frac{1}{2\pi N(\epsilon_F)}\sum_{q\nu}\frac{\gamma_{q\nu}}{\omega_{q\nu}}\delta(\omega-\omega_{q\nu}) \tag{2.50}$$

where $N(\epsilon_F)$ is the electronic density of states at the Fermi level. $\alpha^2F(\omega)$ is important as it permits to evaluate the decrease in the velocity of the electrons due to their interaction with phonons. It should depend on the wave vector k but the average on the Fermi surface is usually enough to describe the system. A transport spectral function can be calculated as $\alpha^2_{tr}F(\omega) = \alpha^2_{out}F(\omega) - \alpha^2_{in}F(\omega)$ where

$$\alpha^2_{out(in)}F(\omega) = \frac{1}{N(\epsilon_F)\langle v_x^2\rangle}\sum_{\nu}\sum_{kjk'j'}|g^{k'-k\nu}_{k'j',kj}|^2 v_x(k)v_x(k^{(\prime)}) \times \delta(\epsilon_{kj}-\epsilon_F)\delta(\epsilon_{k'j'}-\epsilon_F)\delta(\omega-\omega_{k'-k\nu}). \quad (2.51)$$

Here $v_x(k)$ is the Fermi velocity in direction x and $\langle v_x^2\rangle$ is the squared average. Finally the electrical resistivity can be written, in the lowest-order variational approximation for the solution of the Boltzmann equation, as

$$\rho(T) = \frac{\pi\Omega_{cell}k_BT}{N(\epsilon_F)\langle v_x^2\rangle}\int_0^\infty \frac{d\omega}{\omega}\frac{x^2}{\sinh^2 x}\alpha^2_{tr}F(\omega). \quad (2.52)$$

The theory can be expanded to include also spin dependence as in Ref [20]

Chapter 3

Results

In this chapter the results of the present work will be shown. There will be a brief introduction regarding the DFT calculations followed by a more extended section about the resistivity results and a final section regarding the review of a Monte Carlo simulation.

The first part will be used only to cross-check the ab-initio calculations. Good values for the cell parameters will be used to justify the use of pseudopotentials and exchange-correlation functionals. The DFT results of the two codes used, VASP and ABINIT, will be compared between themselves and with additional literature.

The second section will contain the results obtained through several steps of the work and justification for the parameters used in the simulations. After the convergence of the numerical values will have been ensured, a lot of data will follow regarding the resistivity for different systems. Three materials have been considered as a basis, that are aluminium, tungsten and iron. Defected cells are then studied and compared to the bulk calculations, determining the differential resistivity. Other configurations could be easily added if particular data are sought or if certain hypothesis must be verified.

The final Monte Carlo section will contain a possible application of the data that have been accumulated over the span of this work.

3.1 Ab-initio calculations

The calculations have been run using two programs, VASP and ABINIT. The details of the simulations and a brief explanation of the two programs can be found in sections 2.3.4 and 2.3.5. A brief discussion about the results and the problems found during operation will follow as well. It must be reminded that ABINIT works with atomic units whereas VASP uses SI units, however all of the results will be written following the latter convention in order to avoid confusion.

The relaxation of the cells using the two programs yielded similar results. The only material showing some problems is iron, most probably because of its ferromagnetic behaviour. Three materials are shown here, iron, tungsten and aluminium, which are the three used for most of this work, however simulations can be easily and quickly run for any other material.

The results can be considered acceptable compared to the experimental ones

a_0 [Å]	VASP	ABINIT	Experimental [33]
Al	4.0404	4.0495, 4.0542	4.0496
Fe	2.8320	2.8281, 2.8528	2.8665
W	3.1704	3.8780, 3.1600	3.1652

Table 3.1: Lattice parameters for selected elements

and other literature studies. It must be noted that there are two results given for ABINIT simulations, related to two different archives used for the pseudopotentials. The first one was in the same package of the program and was initially used for the calculations. However, the result for tungsten is far off the acceptable margin of error for such calculations, so a new archive was added and used with better outcome. The results for the magnetic moment M in units of Bohr magnetons μ_B are also presented in table 3.2.

M [μ_B]	VASP	ABINIT(GGA pspnc)	ABINIT(GGA paw)	Experimental
Fe	2.20	2.83, 2.83	2.24	2.216 [34]

Table 3.2: Magnetisation of iron

The results obtained with ABINIT do not show a very satisfactory agreement with the experiments and this can possibly affect further results on the conductivity of

iron. The fourth column was added to show that, given a suitable basis it is possible to yield better results. Unfortunately the use of PAW GGA is not yet implemented in DFPT calculations, so the last basis could not be used. Better results can definitely be obtained by using more apt input as it is shown in Ref [20].

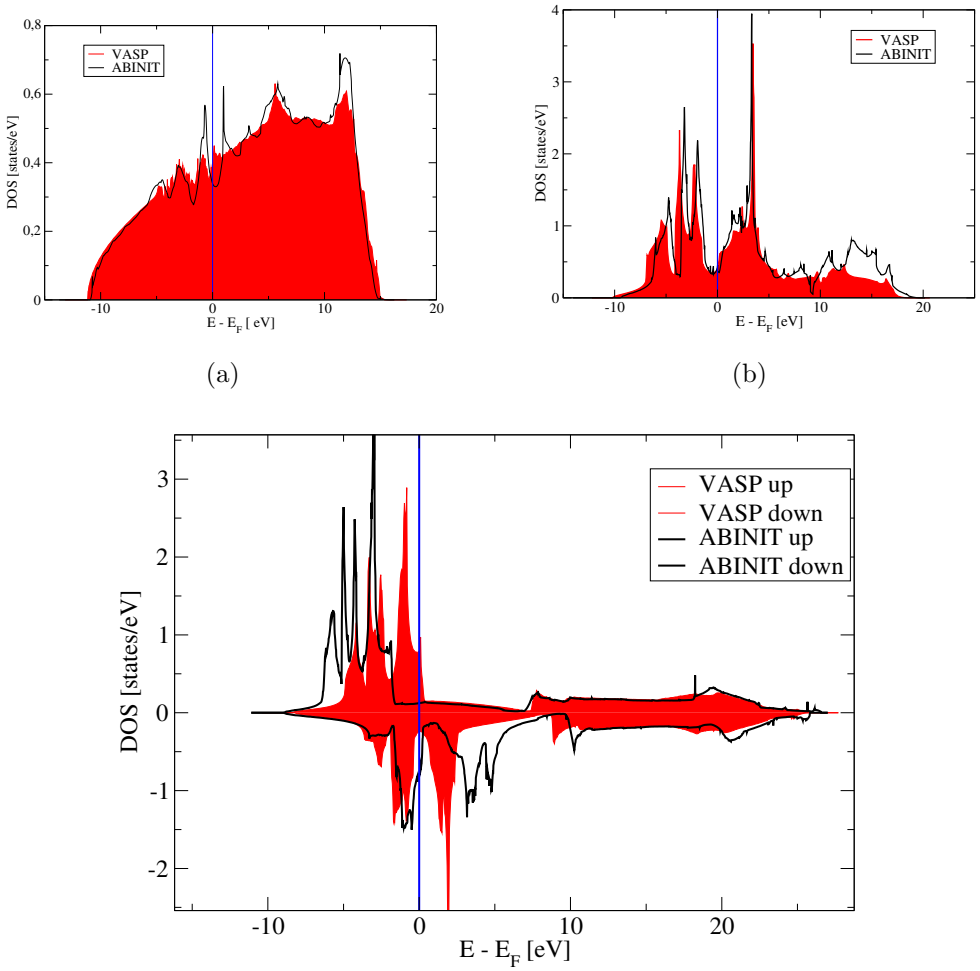

(a) (b)

(c)

Figure 3.1: The density of state of aluminium is presented in Fig. (a), followed by tungsten (b) and iron (c). The red filled area is the DOS obtained with VASP whereas the black lines show the results obtained with ABINIT.

Also the density of states (DOS) can be compared to have a more precise understanding of the differences between the two programs. Figure 3.1 shows a

pretty good agreement in tungsten and aluminium, whereas iron shows a significant shift of the DOS from ABINIT. This shift is reduced when using the PAW GGA in ABINIT as it is used in VASP.

3.2 Transport calculations

In the first part of this section the stability and the convergence of the numerical calculations will be demonstrated, therefore the quantity taken into consideration will be the raw σ/τ from the xxx.trace file output by BoltzTraP. This ensures that no treatment of the data has been yet done. It could also be argued that this preparatory work investigates the validity of the eigenvalues provided by VASP as the σ/τ is calculated directly from these. Other methods have also been used and will then be presented in this section to justify the use of 250 atom supercells. The results will be shown for tungsten but the same simulations and tests have been done also on iron, with similar findings.

Figure 3.2 shows the variation of σ/τ on the number of atoms for the most dense k-point grid that was available, that is 7x7x7, with no symmetry. Three configurations have been chosen as they permit to investigate properly the convergence. All three of them show similar behaviour when increasing the number of atoms and the variation does not exceed 10% from the 128 atoms configuration to the 250 one. It would be useful in this regard to have an additional simulation at 432 to further prove this point but at the moment the computational power required exceeds the one at disposition. Effort will be placed to further investigate this point.

On the 250 atoms configuration, different number of k-points have been investigated, ranging from 3x3x3 to 7x7x7, still with no symmetry. In the x-axis of Figure 3.3 the number of k-points in the IBZ has been reported instead of the k-point grid to have a better understanding of the number of k-points used. The variation between the last two simulations is around 7%. It can also be seen that for a very small number of k-points (14, corresponding to a 3x3x3 grid) the results are not consistent with the other calculations as the σ/τ of the far away divacancy configuration is greater than that of the single vacancy. This would imply that the resistivity of a single vacancy is greater than that of a divacancy, defying logic and all of the other simulations. From this it could possibly be argued that the eigen-

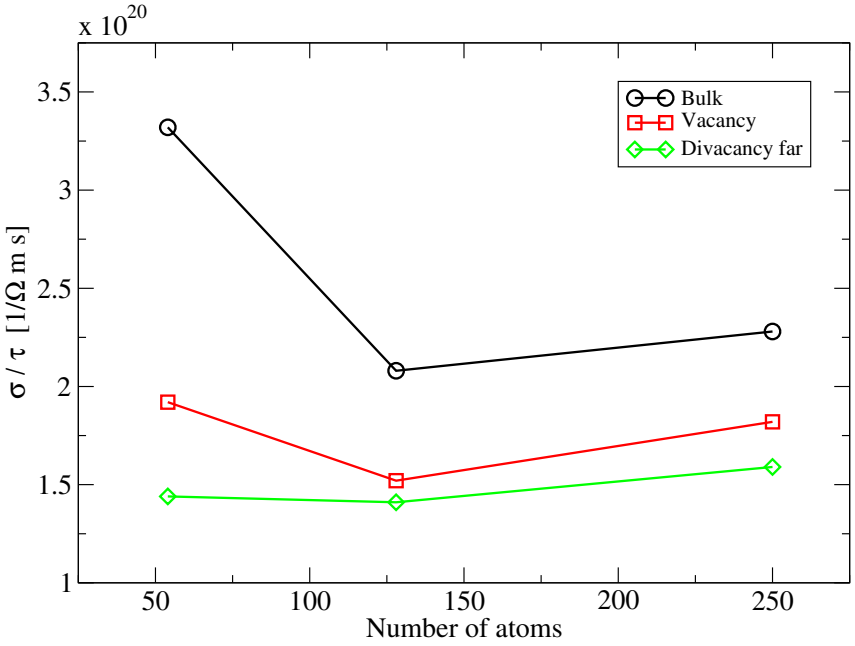

Figure 3.2: Convergence of σ/τ with respect to the number of atoms for a fixed grid of 172 k-points in the IBZ

values calculated with such a low amount of k-points are not reliable for further treatment.

Once the stability and the convergence of the chosen configuration has been proven, other tests have been run in order to check the reliability of the calculations. It is expected, for example, that for a big enough cell in the far away divacancy configuration there should be no interaction between the two vacancies. Therefore the resistivity increase should be equal to a system with a single vacancy but with half the amount of atoms or to twice the resistivity increase due to a single vacancy. Equation 3.1 shows the expected result for such a calculation, that is that the divacancy far configuration is equal to two single vacancies and the resistivity increase is the linear combination of two single vacancies.

$$\Delta\rho_{\text{divac far}}(c) = \Delta\rho_{\text{vac}}(2c) = 2\Delta\rho_{\text{vac}}(c) \tag{3.1}$$

where c identifies the concentration at which the calculations are run, therefore in

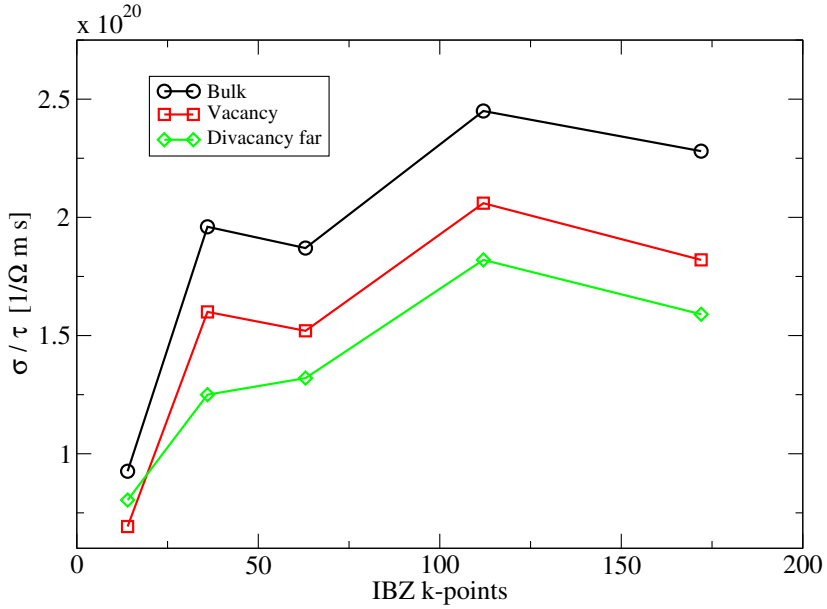

Figure 3.3: Convergence of σ/τ with respect to the number of k-points in the IBZ

this case $c = 1/250$

The results seem to confirm the expected behaviour when comparing 128, 250 and 432 atom supercells, whereas the 54 atoms supercells apparently have much better results than expected. It is rather unreasonable to think that 54 atoms are enough to show the correct predicted behaviour so it is probably a superposition of different causes that bring unexpectedly good results. The fact that the cell is not big enough can also be seen when comparing the charge density of the cells. Despite not giving numerical results, the investigation of the charge density file output by VASP can provide a visual help to clarify the problem at hand. In fact it can be clearly seen that the charge density is well separated in the 250 atoms case whereas for 54 and 128 shows an interaction between the two defects.

It is now possible to make a step forward and compare the bulk simulations to the experimental results, for both ABINIT and BoltzTraP. It must be reminded that for ABINIT no assumptions have been made, whereas for BoltzTraP the density of transport electrons has been chosen to fit the experimental data at a

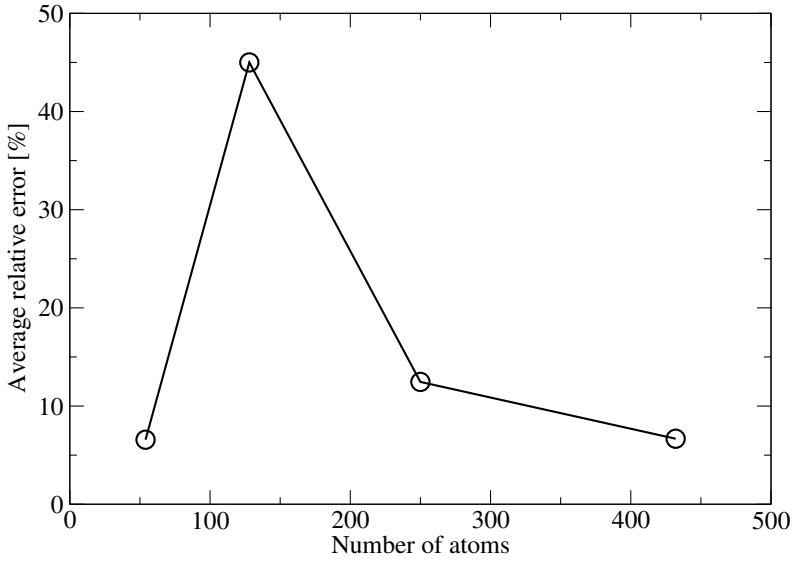

Figure 3.4: Convergence of the average relative error of the difference for increasing number of atoms

given temperature, as explained in section 2.4.3. Both ABINIT and BoltzTraP reproduce extremely well both the aluminium and tungsten cases. For iron the results obtained by ABINIT are not satisfactory, whereas with BoltzTraP there is a better fit. It is evident that more work would be needed for the ABINIT simulation for iron and the first step would be the use of a better pseudopotential as more realistic results have already been obtained in Ref. [20]. Comparing the BoltzTraP resistivity with the one in the cited work it becomes clear that the spins are flipped. The origin of such difference remains unclear but, as it will be seen in the upcoming graphs, it is always consistent for all of the crystallographic configurations that have been studied. It cannot be ruled out that the majority spin has an higher resistivity than the minority one because experiments have not been able to answer this question but more work is needed to verify this result. Within Verstraete's work [20], given the results obtained, an hypothesis has been advanced, that the two spin channels do not simply act as parallel conductors but may interact with each other, therefore reducing the total resistivity to a

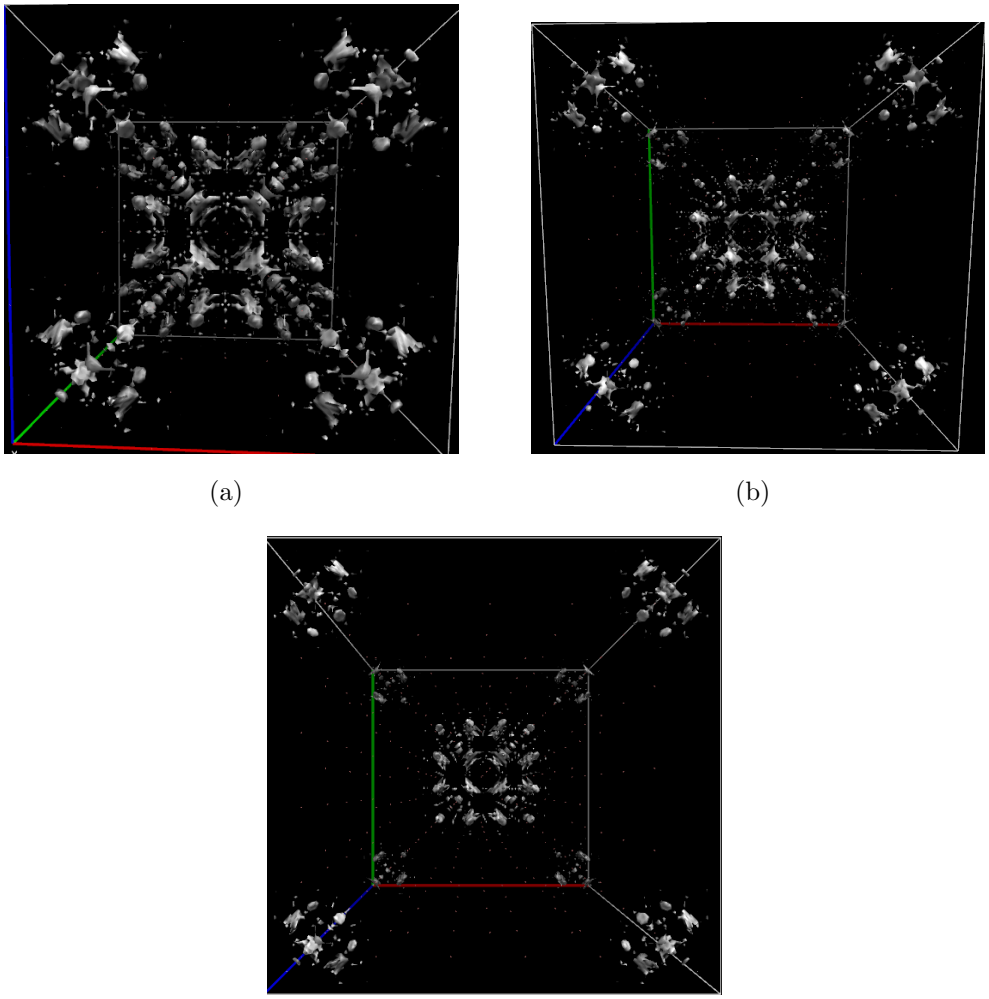

(a) (b)

(c)

Figure 3.5: The charge density of the divacancy far for increasing number of atoms is here presented. It can be noticed how for larger configurations the zone of interaction between the two defects reduces.

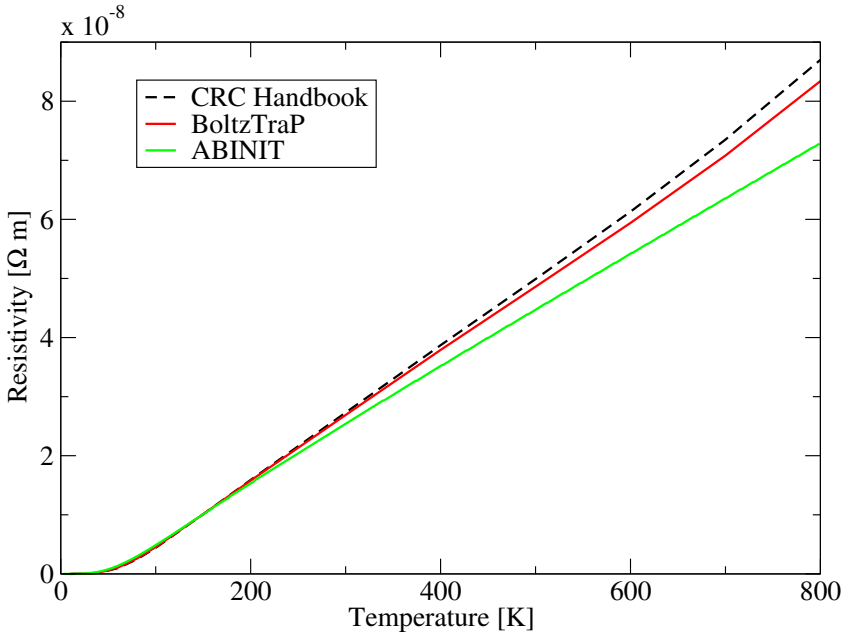

Figure 3.6: Comparison between the resistivity obtained through ABINIT (green line) and BoltzTraP (red line) for aluminium

quantity that is roughly the average of the resistivity of the two spin channels. Such hypothesis has been used within this thesis regarding the resistivity of the various crystallographic configurations.

Given that the results from ABINIT do not have any fitting parameter, it is evident that using such a tool to investigate the objective of the thesis would be preferable. However, as it was stated before, cells bigger than 16 atoms have been found difficult to investigate and therefore BoltzTraP was chosen over ABINIT to study bigger cells. A comparison between the two programs has been made for the simple case of a vacancy in a 16 atoms cell and shows an acceptable agreement at least until room temperature between the two programs. This justifies the use of the combination of VASP and BoltzTraP to investigate bigger cells. For future works it is however advisable to investigate the possibility of using ABINIT for bigger cells, at least for comparison purposes.

Figure 3.10 shows a quick summary of the results that have been obtained

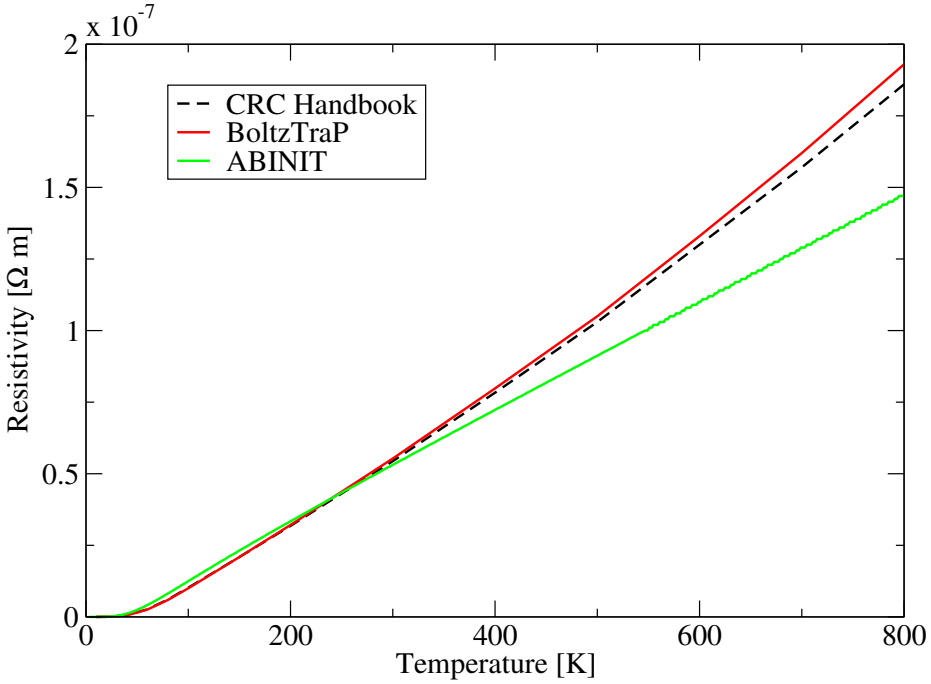

Figure 3.7: Comparison between the resistivity obtained through ABINIT (green line) and BoltzTraP (red line) for tungsten

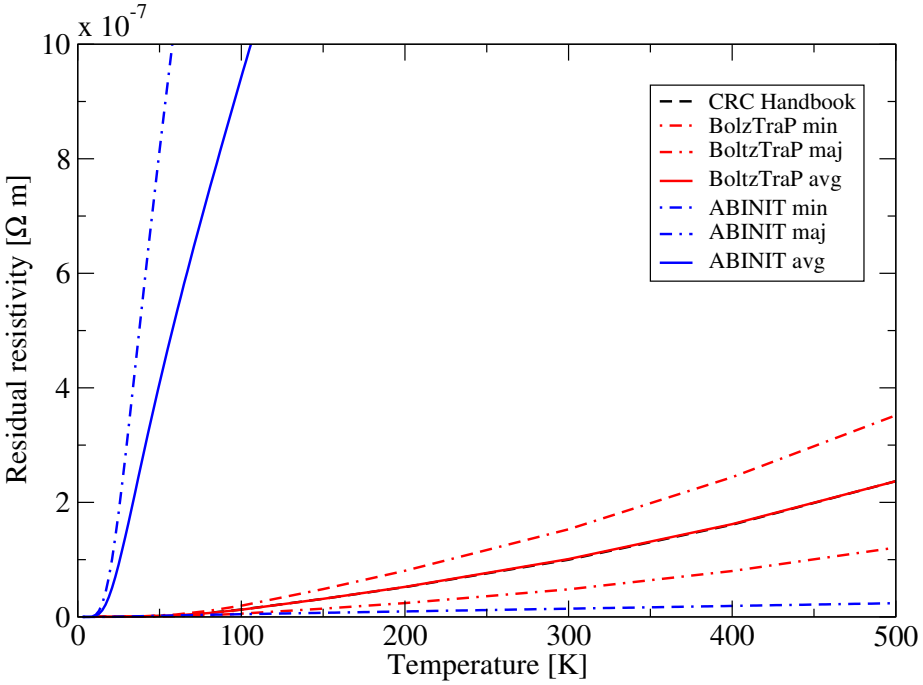

Figure 3.8: Comparison between the resistivity obtained through ABINIT (green line) and BoltzTraP (red line) for iron

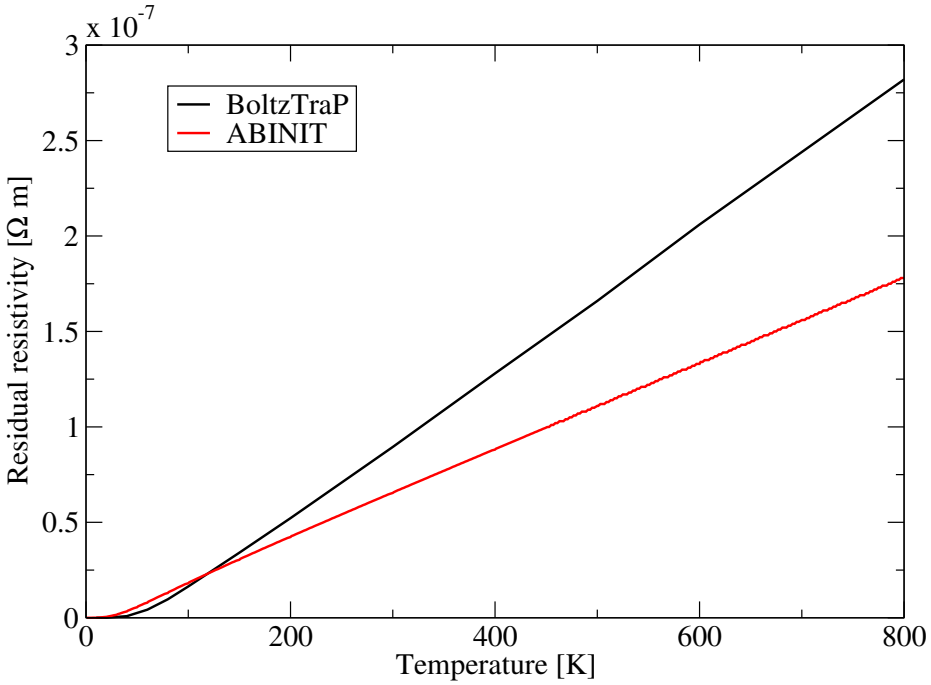

Figure 3.9: Comparison of the residual resistivity of a 16 atoms supercell vacancy for ABINIT and BoltzTraP

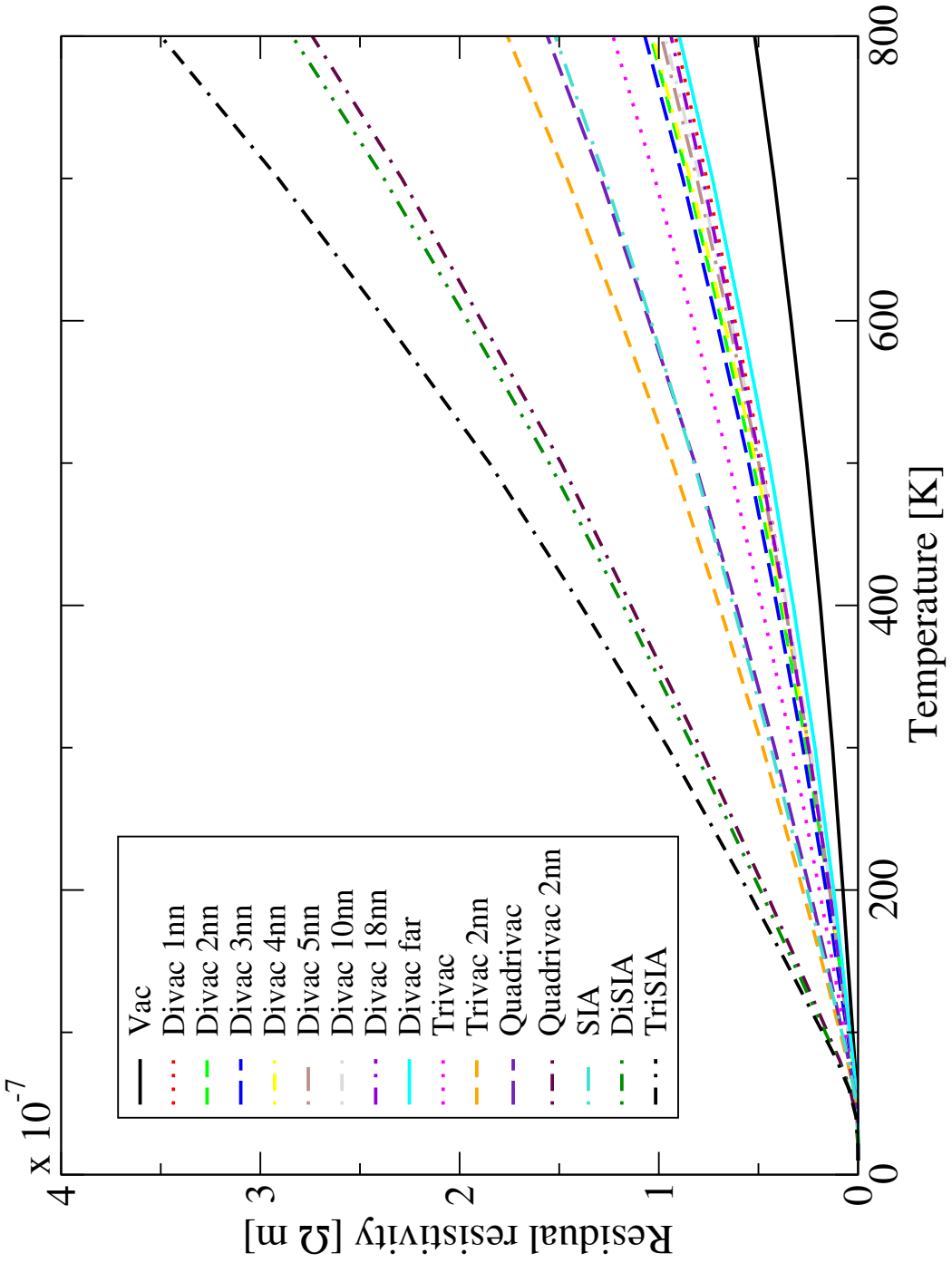

Figure 3.10: Residual resistivity of all the studied configurations for tungsten

for tungsten. All of the most important configurations have been included but it remains difficult to have a clear understanding of each of these. The following figures will clarify the results and possibly give the chance to discuss them.

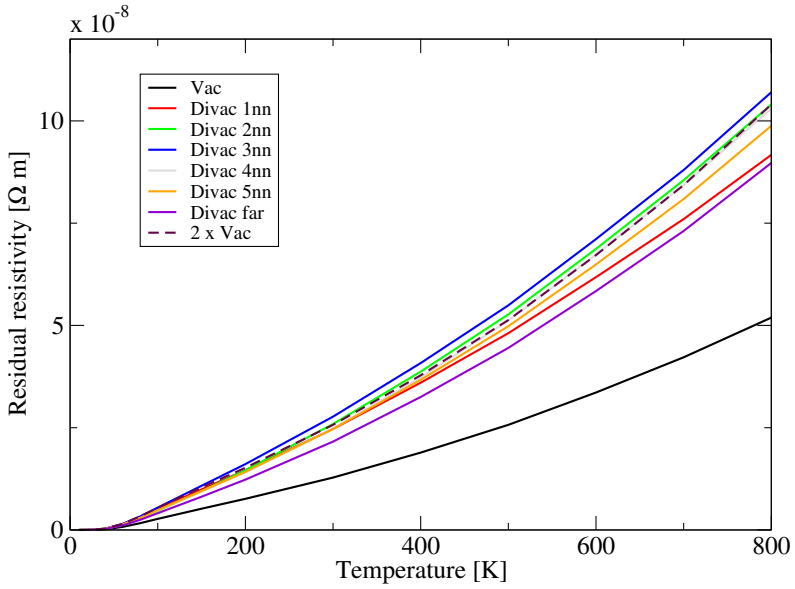

Figure 3.11: Residual resistivity of all the main divacancies for tungsten

In Figure 3.11 several different divacancy configurations have been considered, as shown in Figure 2.3, and the resistivity for each case is compared. One more line has been added which is twice the resistivity of a single vacancy in the 250 atoms case. As it was said before, if no other effect was present it is believed that the far away divacancy should have the same resistivity of twice the single vacancy but it can be seen that there is a slight margin between the two lines. The lack of agreement can possibly be attributed to numerical errors but also to a variation of τ related to the lattice defects which is not taken into consideration in this work. It can be seen that the lowest resistivity is achieved for the 1nn, then it increases till the 3nn and then decreases again for the following configurations. This trend is confirmed for other configurations that have been considered, that is 10nn and 18nn. These configurations are placed along the same direction of the 5nn at increasing distances. The furthest configuration is the far away divacancy

and it is evident in Figure 3.12 how the resistivity is steadily converging towards this value by increasing the distance of the second vacancy.

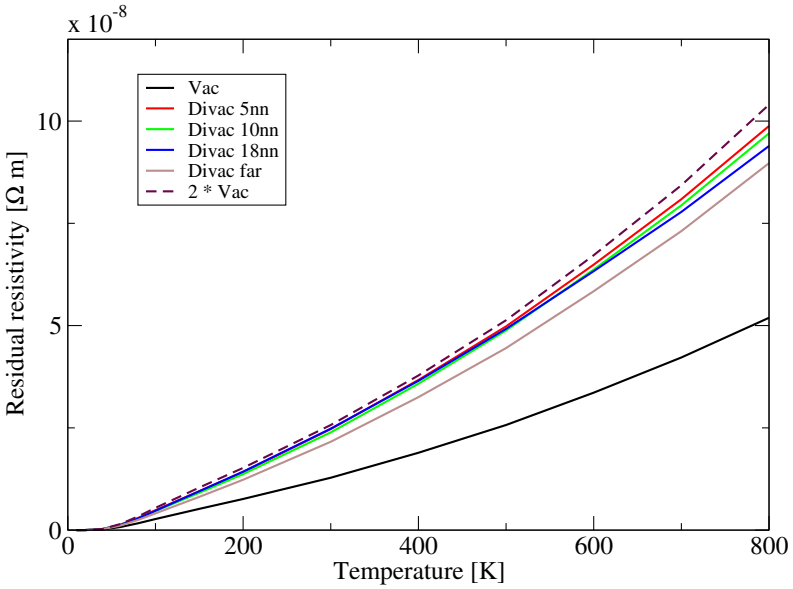

Figure 3.12: Residual resistivity of the distant divacancies for tungsten

The results could be explained by considering that two very close vacancies may interact with each other lowering the total effect on the resistivity. On the other hand it can be seen the that highest resistivity variation does not appear when the two vacancies are most distant from each other but at an intermediate configuration, that is the 3nn. This may be due to a stronger perturbation of the charge density in a small region of space which may increase the total resistivity of the material. It can be noticed how the line representing twice the resistivity of the single vacancy is smaller than the 3nn configuration and approximately equal to the 2nn and 4nn configurations. These results have been confirmed also using a slightly denser grid with a total of 146 k-points.

The same effect can be seen in Figures 3.13 and 3.14 for the trivacancy and quadrivacancy. Figure 3.15 shows the position of the vacancies in the four configurations. The same reasoning as before could be applied to this case. An interesting question that arises is whether the first or the second configuration is the most

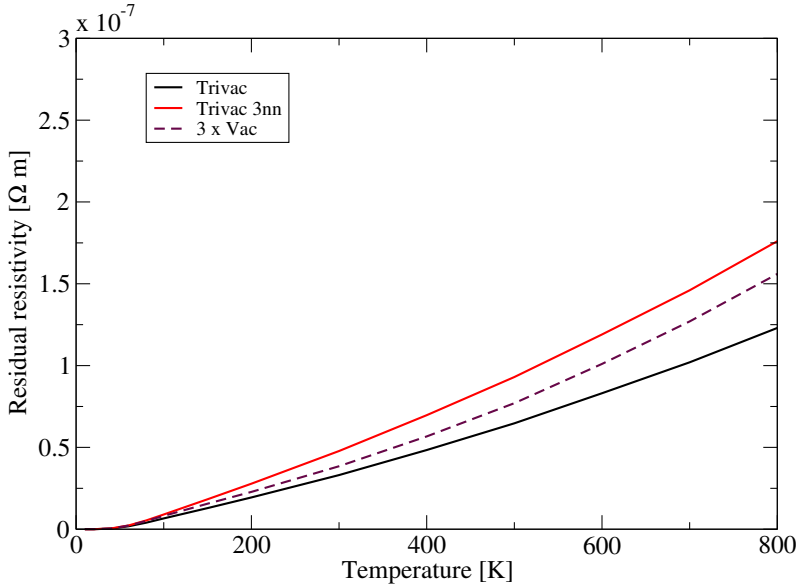

Figure 3.13: Residual resistivity of the trivacancies for tungsten

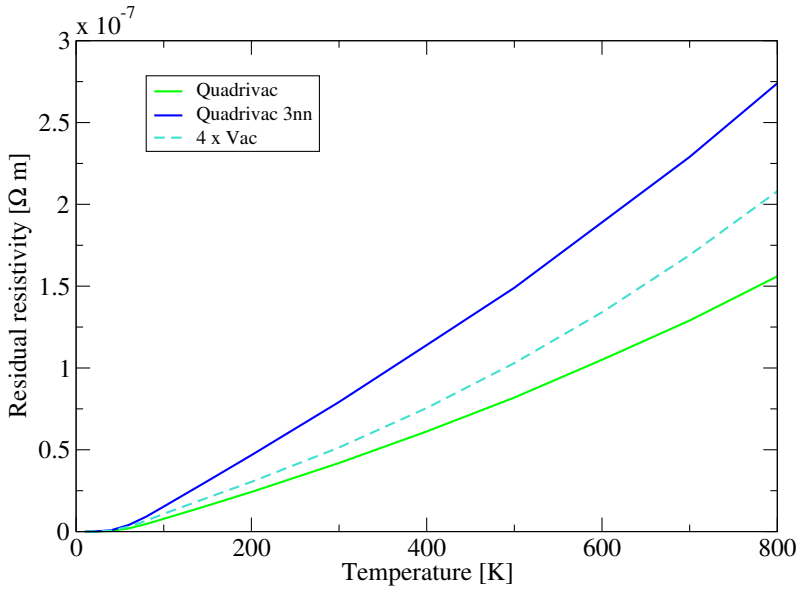

Figure 3.14: Residual resistivity of the quadrivacancies for tungsten

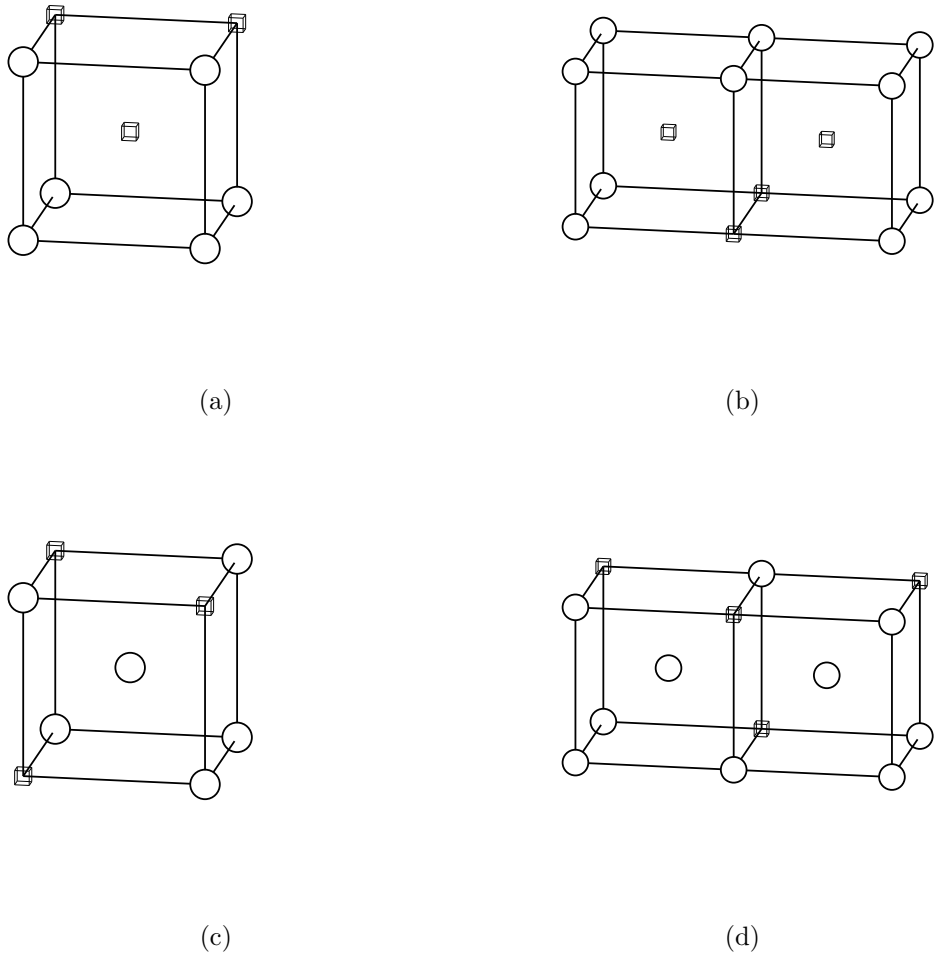

(a) (b)

(c) (d)

Figure 3.15: The configuration for the trivacancies and quadrivacancies is here presented. On top there are the two most close-packed configurations, at the bottom the same clusters but in 3nn position.

stable one or both can be present at the same time. This would be useful to determine the resistivity variation due to the increase and decrease in population of trivacancies and quadrivacancies. Compared to the assumptions made by Fu this would mean that the $\Delta\rho$ associated with each defect is either overestimated or underestimated. It cannot be ruled out, however, that if both defects are present at the same time and in similar numbers, the average value could actually reflect the real variation of the resistivity. A proper weighting of the defect population should be done knowing the formation energies of these configurations and using Boltzmann factors. The self-interstitials show a similarly interesting behaviour.

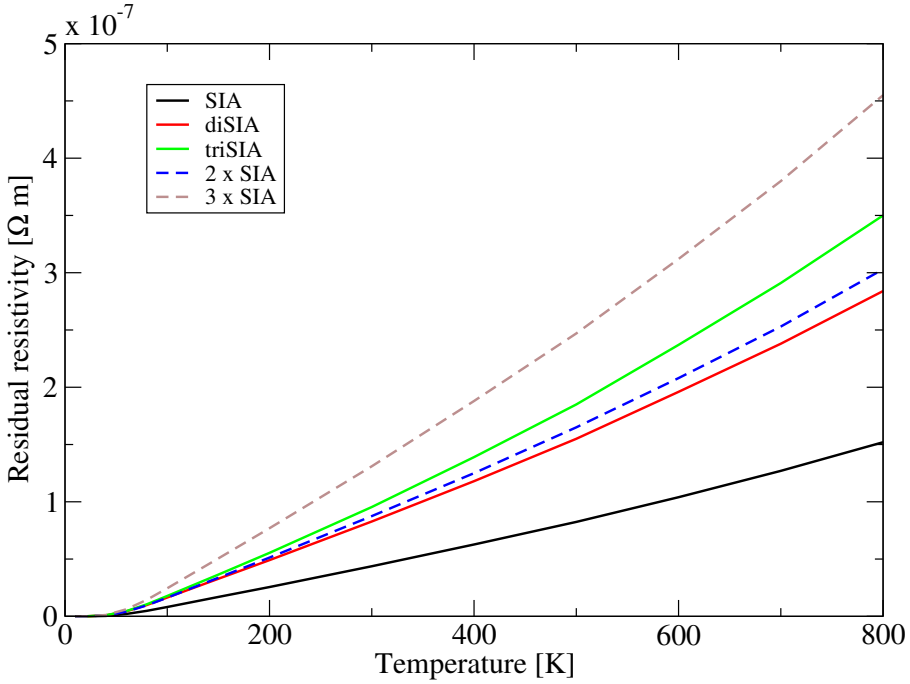

Figure 3.16: Residual resistivity of the trivacancies for tungsten

Their position can be seen in Figure 3.17 and it is evident that they do not show a complete superposition when increasing the number of defects. It can be supposed that it is due to a saturation effect which reduces the impact of several defects concentrated in a small zone. It is also possible to introduce the $\Delta\rho$ of a Frenkel pair by summing the resistivity of a single vacancy with that of a single SIA. This

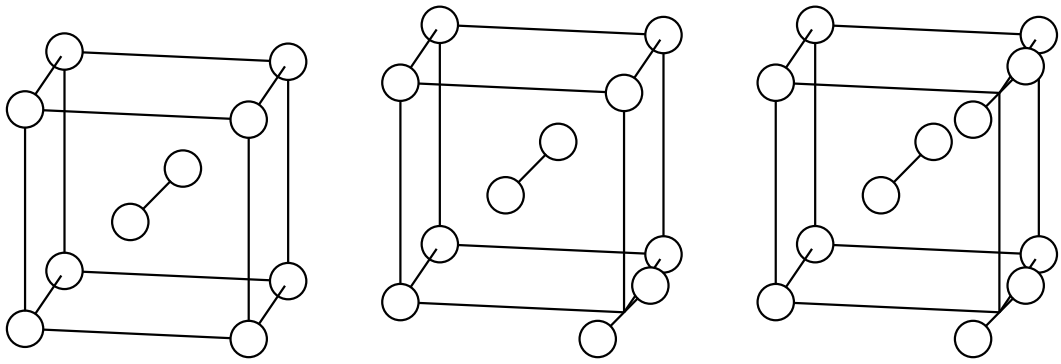

(a) (b) (c)

Figure 3.17: The configuration for the different SIA clusters in tungsten is here presented.

gives useful results because they can also be compared to early measurement for the residual resistivity. In particular it is possible to compare the results to Ref. [6] where an estimate of the residual resistivity of a Frenkel pair is given. The result proposed in the cited work is $\Delta\rho_{\mathrm{FP}} = 1.05 \cdot 10^{-7}\Omega m/at\%$ but this comes from a simplified fitting of the data and possible variations due to errors in measurement are considered, giving a result which is comprised between $7 \cdot 10^{-8}$ and $1.6 \cdot 10^{-7}\Omega m/at\%$. In this work the result obtained for the residual resistivity of a Frenkel pair at 300 K is $1.4 \cdot 10^{-7}\Omega m/at\%$. This result, combined with more recent measurement of the threshold energy in the various directions could yield interesting and quick improvements to the theory.

Configuration	divac 1nn	divac 2nn	divac 3nn	divac 4nn	divac 5nn
Error	1.19%	2.90%	-6.23%	5.14%	1.79%

Table 3.3: The average of the error made by using a linear superposition for divacancies in tungsten

Configuration	trivac	trivac 3nn	quadrivac	quadrivac 3nn
Error	19.3%	-12.5%	40.0%	-31.3%

Table 3.4: The average of the error made by using a linear superposition for trivacancies and quadrivacancies in tungsten

Configuration	diSIA	triSIA
Error	1.97%	29.1%

Table 3.5: The average of the error made by using a linear superposition for self interstitials in tungsten

In Tables 3.3, 3.4 and 3.5 is presented the error committed by considering the resistivity as a linear superposition of defects compared to the resistivity that has been calculated within this work.

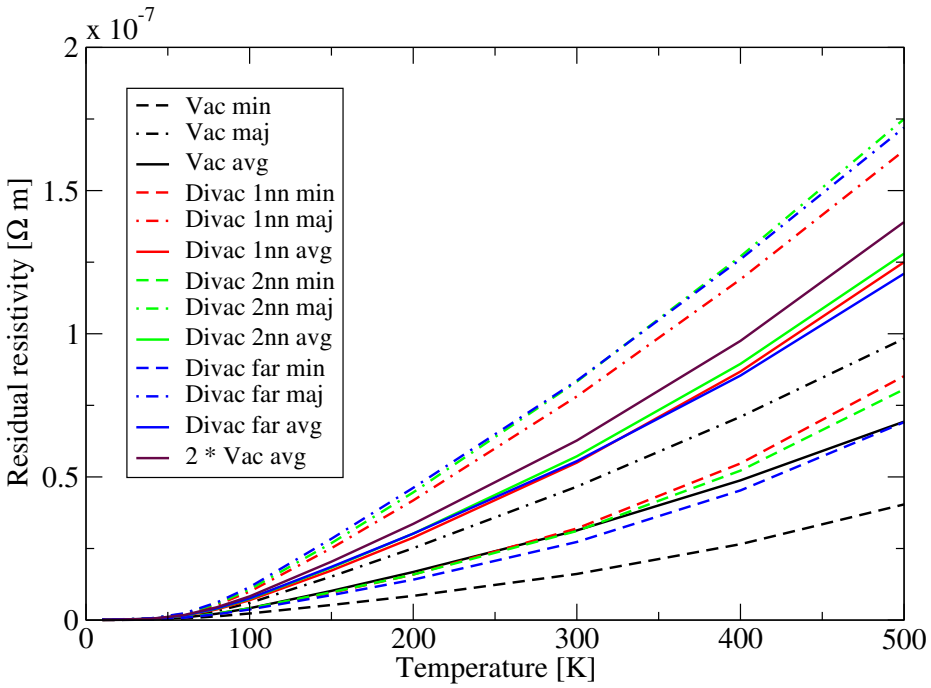

Figure 3.18: Residual resistivity of the divacancies for iron

For iron fewer configurations have been run due to time limitations on the work. However, it has been decided to focus on those configurations which may yield the most interesting results. Figure 3.18 and 3.19 show the obtained resistivities for vacancies and interstitials. The dashed lines represent the majority and minority spin, whereas the thicker solid line represents the average of the two spins and is the

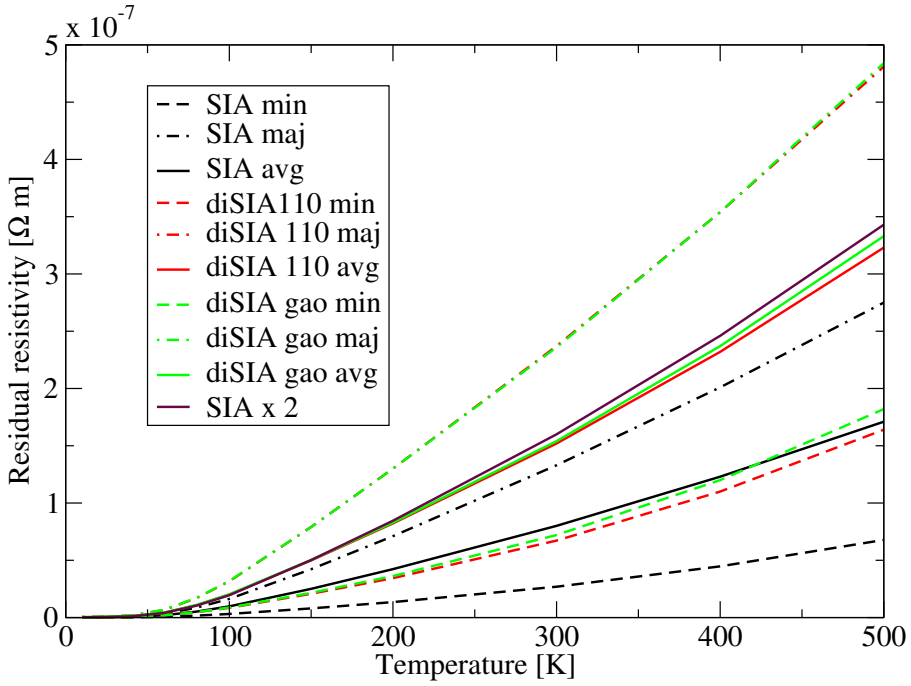

Figure 3.19: Residual resistivity of the SIAs for iron

one result that has been compared. It can be seen that the superposition is roughly respected for both cases. For the divacancies the position of the second vacancy with respect to the first does not appear to influence the resistivity. Similarly, the two di-SIA configurations yield comparable results. It is then possible to produce a table similar to the previous one, showing the error done by using linear superposition instead of exactly calculated resistivities. The major missing configuration is the tri-SIA which could be easily added to improve the current work.

Configuration	divac 1nn	divac 2nn	divac far	110 diSIA	110 Gao diSIA
Error	18.5%	10.2%	10.3%	6.30%	6.14%

Table 3.6: The average of the error made by using a linear superposition for all the configurations in iron

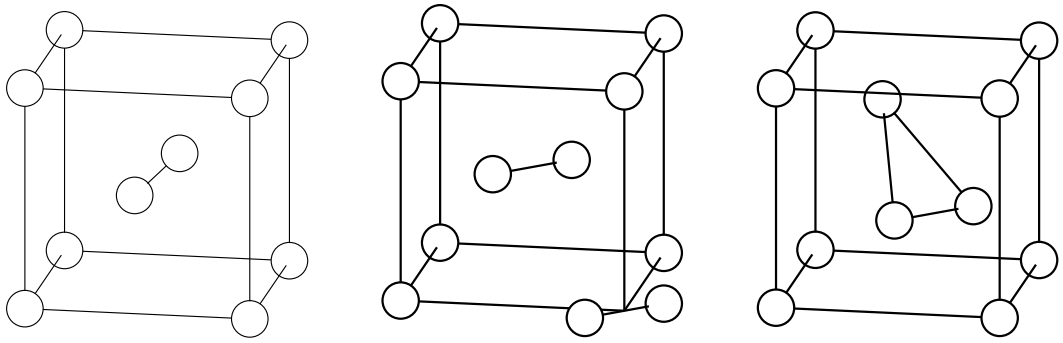

(a) (b) (c)

Figure 3.20: The configuration for the different SIA clusters in iron is here presented.

In this case too there is a very good agreement between the experimental and the calculated values for the residual resistivity as in Ref [7] the value associated with the residual resistivity of a Frenkel pair is $\Delta\rho_{\mathrm{FP}} = 3 \pm 0.5 \cdot 10^{-7}\Omega m/at\%$ and the value obtained from the simulations is $2.79 \cdot 10^{-7}\Omega m/at\%$.

3.3 Kinetic Monte Carlo

The results that have been obtained until now can be used to complement other simulations done in the past or be the base for further research on the topic of isochronal annealing in the future. In this case a new analysis of the data obtained by Fu and co-workers [9] can be done and possibly lead to new conclusions. The data regarding the number of defects at increasing temperatures were extracted and two set of results were then computed and compared. The first set follows the prescriptions from Fu and the total resistivity has been calculated as a function of the number of defects, neglecting their structure, as

$$\rho_{\mathrm{TOT}} = c_{\mathrm{v}} \cdot \Delta\rho_{\mathrm{v}} + c_{\mathrm{SIA}} \cdot \Delta\rho_{\mathrm{SIA}} \tag{3.2}$$

where c_{x} indicates the concentration of vacancies or self-interstitials and $\Delta\rho_{\mathrm{x}}$ the residual resistivity associated to that defect as calculated in this work. In the second set the total resistivity was calculated considering the values computed within this thesis where available and introducing a saturation effect where the

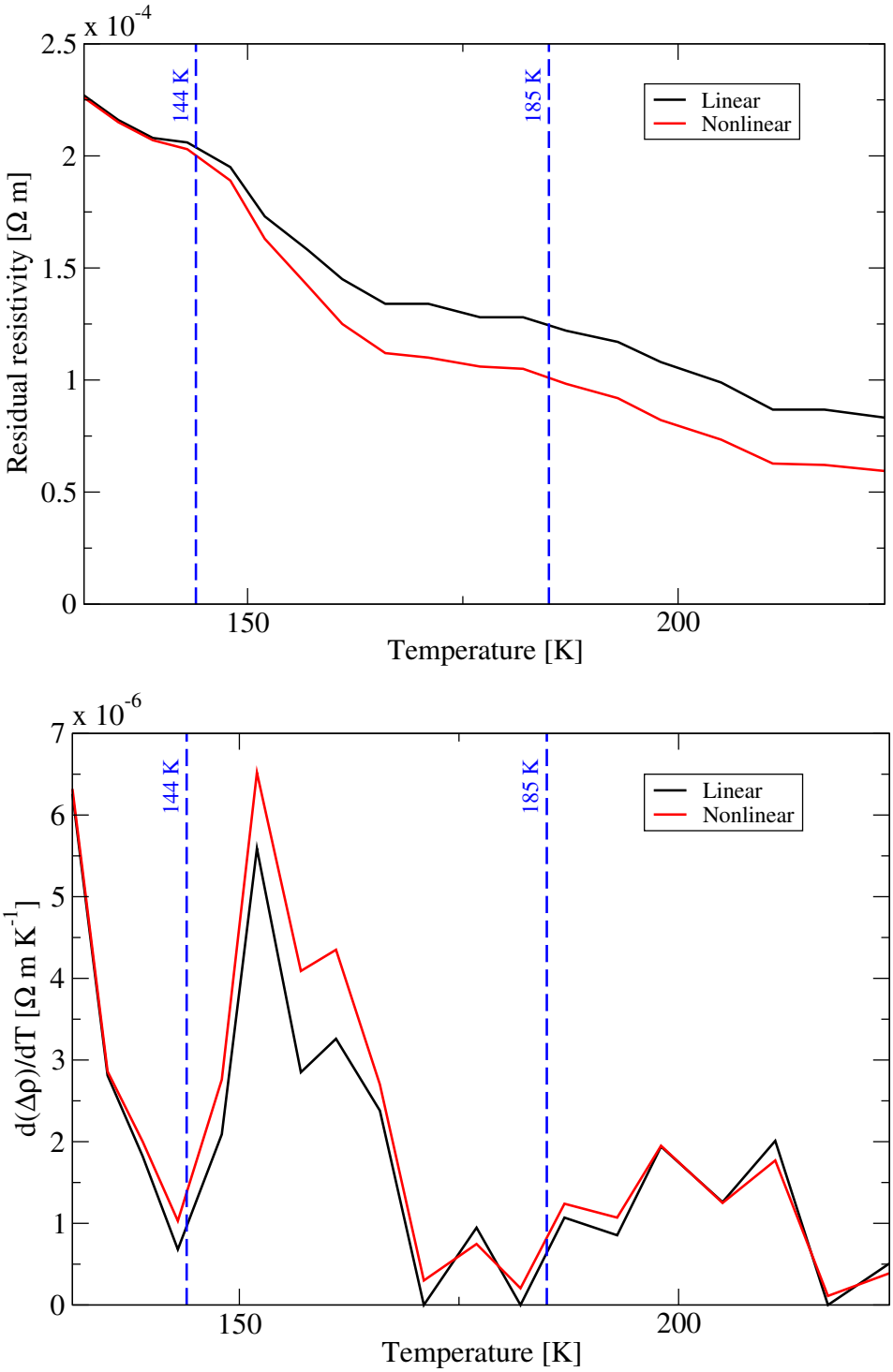

Figure 3.21: In the two plots it is possible to see how the resistivity varies depending on the model used. The linear model is a representation of the results obtained by Fu and coworkers [9] with actual values for the residual resistivity of vacancies and SIAs. On top the total residual resistivity is presented and on the bottom the derivative of the residual resistivity with respect to the temperature. The dashed lines represents the experimental temperatures at which the peaks are observed. The original data already present a shift which is kept in the non-linear model.

results were not available. This leads to consider the resistivity of a tri-SIA as the superposition of three self-interstitials multiplied by a factor of 0.7 due to the saturation of the resistivity. For the SIA-clusters a factor of 0.6 has been used but the lack of knowledge regarding the dimension of the clusters has provided a small uncertainty over the results. The formula used can be written as

$$\rho_{\mathrm{TOT}} = c_{1\mathrm{v}} \cdot \Delta\rho_{1\mathrm{v}} + c_{1\mathrm{SIA}} \cdot \Delta\rho_{1\mathrm{SIA}} + c_{2\mathrm{SIA}} \cdot \Delta\rho_{2\mathrm{SIA}} + c_{3\mathrm{SIA}} \cdot 3\Delta\rho_{1\mathrm{SIA}} \cdot 0.7 + c_{\mathrm{nSIA}} \cdot n\Delta\rho_{1\mathrm{SIA}} \cdot 0.6 \quad (3.3)$$

where n is the average number of SIA in the cluster, calculated assuming that the total number of vacancies and interstitials remains the same.

The temperature range between 130 and 220 K has been isolated as it is the most interesting for this work. At lower temperatures mainly single vacancies and single interstitials exist, therefore no difference can be observed between the two models. At higher temperatures vacancy clusters begin to form but their number remains low and does not influence appreciably the resistivity, whereas the SIAs are connected into bigger clusters whose dimension is unknown. In between the vacancies continue to exist as single defects, as they are not yet able to move, whereas the interstitial begin the formation of small clusters and their behaviour influences noticeably the total resistivity. The results can be seen in Fig. 3.21 and show that a shift in the resistivity is evident when comparing the two cases. The derivative, presented on the bottom of Fig 3.21, shows a taller peak around 152 K and roughly the same absolute value around 200 K. This second peak would probably vary if the composition of the SIA clusters was known. The relative difference between the two results at 152 K is around 17%.

Chapter 4

Conclusions

The objective of the work was to determine the variation of the residual resistivity of the defects depending on their configuration. In other works it was assumed that clusters of defects behaved as the sum of the defects that composed them, so a tri-SIA had the same residual resistivity as the sum of three SIAs. However, the possibility to investigate the correctness of this assumption existed had to be attempted. Therefore a combination of DFT simulations and electron transport codes has been used in order to investigate the behaviour of the residual resistivity for different defects.

Two methods were proposed, both relying on DFT calculations coupled with electron transport codes based on the semi-classical Boltzmann theory. In the first method ABINIT was used for both parts as it is able to perform both DFT and DFPT calculations, necessary to investigate the resistivity. The second method relies on DFT simulations performed with VASP and then coupled with BoltzTraP, which makes use of the eigenvalues output from VASP to calculate several transport-related quantities.

ABINIT has shown great potential regarding the calculations of the transport coefficient as the results obtained show a good agreement with the experimental ones without the use of any fitting parameter. However, the program has shown computational limits when bigger cells were used and the investigation of large defected cells was thus stopped in favour of the use of VASP and BoltzTraP. Small cells were still investigated in order to validate the results obtained through the other method. VASP and BoltzTraP, on the other hand, needed a fitting

parameter, the density of conduction electrons, in order to replicate correctly the base experimental data. However, all the results that have been presented do not rely on this parameter as the difference between the resistivities of two different configurations depends solely on the initial σ/τ which is an output of the program.

The focus of the research was put on two materials of interest, iron and tungsten. Both of them were chosen because of their application (present and future) in the nuclear industry, fission and fusion, and therefore are subject to an important amount of radiation. Tungsten has also been used to test the whole method before applying it to iron which, being ferromagnetic, is more complex. Some work has also been done in order to process iron with BoltzTraP, which at first was not possible.

Although the results were expected to be only qualitatively correct, a satisfactory agreement has been found regarding the calculated values of the residual resistivity of a Frenkel pair and the literature, hinting that they may be also quantitatively accurate.

The calculations have revealed that considering a pure linear superposition for cluster of defects is not completely correct. It is evident that other effects take place which change the residual resistivity of the clusters. Differences can be noticed also depending on the relative position of the defects showing either a saturation or a strengthening effect.

The results obtained with iron have been used to investigate how previous works on the topic would be affected by the outcome of this thesis. It has been shown that there would be a noticeable difference in the absolute values of the residual resistivity but the general behaviour would be conserved. More could be done, however, if all the information related to the referenced simulation was known.

The objectives set at the beginning of the work have been met and they cleared the path to a deeper understanding of the topic. The results can be considered to be at least qualitatively correct and set a reference for future work. There are several areas for improvement but in general it can be said that this has been a good first step and has solved many of the problems encountered.

A quick progress could be done by expanding the already available results, increasing the type and number of defects analysed and possibly extending the same results to other materials. A program could be written to avoid the painful

process of copy paste which is now necessary to treat each single set of results. Also a guide should be added so to make it easier to learn how to use BoltzTraP and couple it properly with VASP.

A second improvement, which would probably dramatically decrease the time needed for such simulations, is related to the exploitation of the symmetries in BoltzTraP. VASP is able to reduce the time and power needed for a calculation by correctly exploiting the symmetry of the system at hand. However, it has been impossible to similarly exploit the symmetry in BoltzTraP. The solution adopted within this work was to run the VASP simulations with a very low symmetry and let BoltzTraP run without using the symmetries of the system. This has had an important impact on the amount of time and power needed by VASP to run the simulations. It is evident that, if the symmetries could have been correctly exploited, more work could be done, possibly even with bigger cells, clusters and a denser k-point grid.

The possibility of using ABINIT to calculate the residual resistivity for bigger cells should be investigated. The bulk calculations have provided very good results and it is expected that the resistivity calculation of defected configurations would be equally precise. 54 atoms cells would probably be enough to investigate single defects, whereas bigger cells, 250 atoms were the standard in VASP and BoltzTraP, would be needed to study clusters of defects. Otherwise VASP could be modified in order to do DFPT calculations to avoid altogether the use of BoltzTraP.

A final possibility of improvement concerns the correctness of the models used. The Drude model for the calculation of τ could possibly be replaced. It is expected and predicted by certain models that τ may vary depending on the lattice and the defects in it. However, it should be kept in mind that increasing the complexity may not yield correct results as the Boltzmann theory at the base already has some known flaws. It would also be of extreme interest to study analytically how the majority and the minority spin channels interact in iron and other ferromagnetic materials.

Bibliography

[1] LK Mansur et al. "Materials needs for fusion, Generation IV fission reactors and spallation neutron sources–similarities and differences". In: *Journal of Nuclear Materials* 329 (2004), pp. 166–172.

[2] A Alamo et al. "Assessment of ODS-14% Cr ferritic alloy for high temperature applications". In: *Journal of Nuclear Materials* 329 (2004), pp. 333–337.

[3] Frank Bergner et al. "Critical assessment of Cr-rich precipitates in neutron-irradiated Fe–12at% Cr: Comparison of SANS and APT". In: *Journal of Nuclear Materials* 442.1 (2013), pp. 463–469.

[4] MK Miller, BD Wirth, and GR Odette. "Precipitation in neutron-irradiated Fe–Cu and Fe–Cu–Mn model alloys: a comparison of APT and SANS data". In: *Materials Science and Engineering: A* 353.1 (2003), pp. 133–139.

[5] Andreas Ulbricht et al. "SANS response of VVER440-type weld material after neutron irradiation, post-irradiation annealing and reirradiation". In: *Philosophical Magazine* 87.12 (2007), pp. 1855–1870.

[6] F Maury et al. "Frenkel pair creation and stage I recovery in W crystals irradiated near threshold". In: *Radiation Effects* 38.1-2 (1978), pp. 53–65.

[7] F. Maury et al. "Anisotropy of defect creation in electron-irradiated iron crystals". In: *Phys. Rev. B* 14 (12 Dec. 1976), pp. 5303–5313.

[8] T Jourdan et al. "Direct simulation of resistivity recovery experiments in carbon-dopedα-iron". In: *Physica Scripta* 2011.T145 (2011), p. 014049.

[9] Chu-Chun Fu et al. "Multiscale modelling of defect kinetics in irradiated iron". In: *Nature materials* 4.1 (2005), pp. 68–74.

[10] Emmanuel Clouet and Alain Barbu. "Using cluster dynamics to model electrical resistivity measurements in precipitating AlSc alloys". In: *Acta materialia* 55.1 (2007), pp. 391–400.

[11] F Knider, J Hugel, and AV Postnikov. "Ab initio calculation of dc resistivity in liquid Al, Na and Pb". In: *Journal of Physics: Condensed Matter* 19.19 (2007), p. 196105.

[12] Pier Luigi Silvestrelli, Ali Alavi, and Michele Parrinello. "Electrical-conductivity calculation in ab initio simulations of metals: Application to liquid sodium". In: *Physical Review B* 55.23 (1997), p. 15515.

[13] Monica Pozzo, Michael P Desjarlais, and Dario Alfè. "Electrical and thermal conductivity of liquid sodium from first-principles calculations". In: *Physical Review B* 84.5 (2011), p. 054203.

[14] Pier Luigi Silvestrelli. "No evidence of a metal-insulator transition in dense hot aluminum: A first-principles study". In: *Physical Review B* 60.24 (1999), p. 16382.

[15] Vanina Recoules and Jean-Paul Crocombette. "Ab initio determination of electrical and thermal conductivity of liquid aluminum". In: *Physical Review B* 72.10 (2005), p. 104202.

[16] Dario Alfè, Monica Pozzo, and Michael P Desjarlais. "Lattice electrical resistivity of magnetic bcc iron from first-principles calculations". In: *Physical Review B* 85.2 (2012), p. 024102.

[17] Henrik Löfås et al. "Transport coefficients in diamond from ab-initio calculations". In: *Applied Physics Letters* 102.9 (2013), p. 092106.

[18] Siham Ouardi et al. "Electronic structure and optical, mechanical, and transport properties of the pure, electron-doped, and hole-doped Heusler compound CoTiSb". In: *Physical Review B* 86.4 (2012), p. 045116.

[19] Ji Young Kim et al. "Abnormal drop in electrical resistivity with impurity doping of single-crystal Ag". In: *Scientific reports* 4 (2014).

[20] Matthieu J Verstraete. "Ab initio calculation of spin-dependent electron–phonon coupling in iron and cobalt". In: *Journal of Physics: Condensed Matter* 25.13 (2013), p. 136001.

[21] Neil W Ashcroft and N David Mermin. *Solid State Physics*. 1976.

[22] Gary S Was. *Fundamentals of radiation materials science: metals and alloys*. Springer Science & Business Media, 2007.

[23] Max Born and Robert Oppenheimer. "Zur quantentheorie der molekeln". In: *Annalen der Physik* 389.20 (1927), pp. 457–484.

[24] NM Harrison. "An introduction to density functional theory". In: *NATO SCIENCE SERIES SUB SERIES III COMPUTER AND SYSTEMS SCIENCES* 187 (2003), pp. 45–70.

[25] Pierre Hohenberg and Walter Kohn. "Inhomogeneous electron gas". In: *Physical review* 136.3B (1964), B864.

[26] Walter Kohn and Lu Jeu Sham. "Self-consistent equations including exchange and correlation effects". In: *Physical Review* 140.4A (1965), A1133.

[27] David M Ceperley and BJ Alder. "Ground state of the electron gas by a stochastic method". In: *Physical Review Letters* 45.7 (1980), p. 566.

[28] John P Perdew, Kieron Burke, and Matthias Ernzerhof. "Generalized gradient approximation made simple". In: *Physical review letters* 77.18 (1996), p. 3865.

[29] David Vanderbilt. "Soft self-consistent pseudopotentials in a generalized eigenvalue formalism". In: *Physical Review B* 41.11 (1990), p. 7892.

[30] PB Allen. "Electron Transport". In: *Contemporary Concepts of Condensed Matter Science* 2 (2006), pp. 165–218.

[31] Georg KH Madsen and David J Singh. "BoltzTraP. A code for calculating band-structure dependent quantities". In: *Computer Physics Communications* 175.1 (2006), pp. 67–71.

[32] S Yu Savrasov and D Yu Savrasov. "Electron-phonon interactions and related physical properties of metals from linear-response theory". In: *Physical Review B* 54.23 (1996), p. 16487.

[33] William M Haynes. *CRC handbook of chemistry and physics*. CRC press, 2013.

[34] J Callaway and CS Wang. "Energy bands in ferromagnetic iron". In: *Physical Review B* 16.5 (1977), p. 2095.